UNIVERSITY OF CALIFORNIA SAN DIEGO

Handheld Robotic Catheter for Intraluminal Instrument Mobility

A thesis submitted in partial satisfaction of the
requirements for the degree
Master of Science

in

Electrical and Computer Engineering (Medical Devices and Systems)

by

Harleen Singh

Committee in charge:

Professor Michael Yip, Chair
Professor Todd Coleman
Professor Karcher Morris

2021

The thesis of Harleen Singh is approved, and is acceptable in quality and form for publication on microfilm and electronically.

University of California San Diego

2021

DEDICATION

To my family for all their love and support and for inspiring me to pursue projects that I love.

To my friends, professors, and mentors throughout the years that have allowed me to learn and grow as an engineer and have inspired me to pursue exciting, impactful projects.

TABLE OF CONTENTS

LIST OF FIGURES

LIST OF TABLES

ACKNOWLEDGEMENTS

Thank you to Professor Yip for supporting me throughout the course of this project and for giving me the freedom and autonomy to develop this project over the last two years. I appreciate his diligence, patience, and willingness to allow this project to progress over time in many different directions. This thesis would not have been possible if not for his guidance and support.

Thank you to Barbara Durrant, Parker Pennington, and Nicole Ravida from the San Diego Safari Park for your assistance with this project. I appreciate the support and guidance you provided me with. Thank you as well to Kim Sover and Anthony Jiang for your contributions to this project. I appreciate all the work you have done to progress this project forward.

Thank you also to Florian Richter and Dimitri Schreiber for mentoring me throughout the course of this project. The advice and assistance you both provided me with is invaluable, and I cannot thank you enough for your kindness, patience, and willingness to assist me.

I would also like to thank everyone in the Advanced Robotics and Controls Lab for all of the entertaining conversations, debates, and ECE coffee hours. I learned so much from everyone in this lab, and I am grateful for all of the connections I was able to make during my time in this lab.

VITA

2019	B. S. in Nanoengineering, University of California San Diego
2019	B. A. in International Business, University of California San Diego
2019-2020	Research and Development Engineer I, University of California San Diego
2021	M. S. in Electrical and Computer Engineering, University of California San Diego

ABSTRACT OF THE THESIS

Handheld Robotic Catheter for Intraluminal Instrument Mobility

by

Harleen Singh
Master of Science in Electrical and Computer Engineering (Medical Devices and Systems)

University of California San Diego, 2021

Professor Michael Yip, Chair

In this work, we present a portable, lightweight, modular, and flexible handheld robotic catheter designed to assist surgeons in performing surgical procedures by providing increased imaging capabilities, flexibility, and modularity. This is the first handheld roboticized catheter of its kind capable of navigating complex, convoluted, and highly constrained unseen environments with dexterity. The device has been tested in a variety of environments, both seen and unseen, with varying levels of complexity, beginning with simple anatomical models with the goal of moving toward *in vivo* experiments.

Chapter 1

Introduction

In recent years, there has increasingly been a push to incorporate robotics into medical procedures and diagnostics, aiming to make them safer and more effective at addressing ailments either by replacing aspects of surgery typically performed by surgeons or to better assist surgeons in ensuring positive outcomes. Within this field of surgical or medical robotics, many have attempted to treat or diagnose lung cancer.

The central application of this work centers around bronchoscopy for lung cancer detection, but we expect to adapt the device outlined in this work for a variety of additional endoscopic procedures.

This chapter will serve to motivate the work and will introduce the relevant information necessary for detailing the novel device covered in this thesis. It will be divided into the following sections:

1. An overview of lung cancer and its mortality rates.
2. An overview of a common methodology used to treat lung cancer.
3. Previous works who have used variations of this methodology to diagnose lung cancer or select other catheter-based procedures to diagnose or treat various maladies.
4. The contributions we are proposing to add to the medical field through the work outlined in this thesis.

1.1 Lung Cancer

As of 2015, lung cancer was the leading cancer-related cause of death in men worldwide and the second leading cause of death in women worldwide. Lung cancer is exceedingly prevalent in older populations, primarily occurring at higher rates in older populations as compared to younger people. As of 2010, the statistics showed that in the United States, 585.9 out of 100,000 men ages 85-89 and 365.8 out of 100,000 women ages 75-79 showed signs for lung cancer, while only 1.3 per 100,000 men and 1.4 per 100,000 women ages 30–34 showed signs of lung cancer. Moreover, the survival rate among lung cancer patients is fairly low, with a rate of 18% for those diagnosed between 2003-2009 [14]. This percentage is largely correlated with the stage at which the lung cancer is detected. Detection at early stages via positive lung biopsy can allow for improved outcomes as intervention can be taken early on to prevent the cancer from spreading or developing in magnitude.

A diagnostic treatment that is successful at detecting for early stage lung cancers is transbronchial lung biopsy. In a transbronchial lung biopsy, a piece of lung tissue is removed using forceps, or surgical scissors, which are passed through the working channel of a bronchoscope. A figure detailing this procedure using a flexible endoscope can be seen in Figure 1.1.

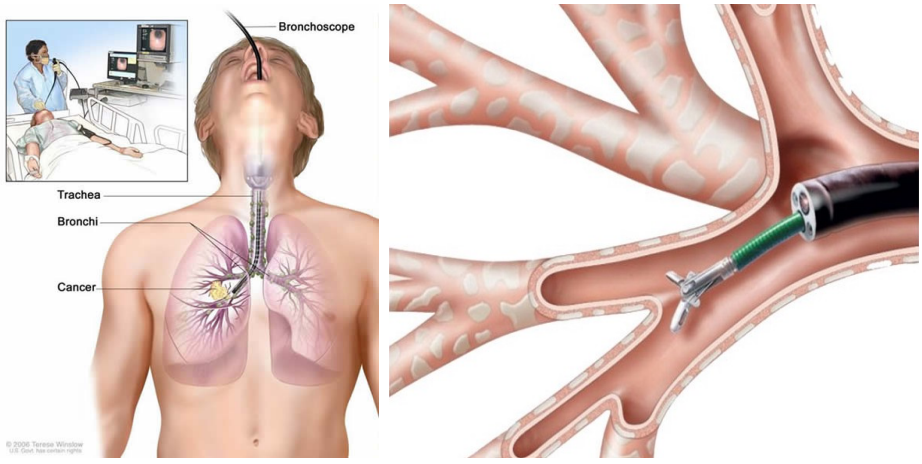

Figure 1.1: A visual representation of a transbronchial lung biopsy using a flexible endoscope [1][2]

1.2 Bronchoscopy

To detect lung cancer at earlier stages, specialists can perform lung biopsies to determine whether inflamed or otherwise suspicious tissues are cancerous in nature by removing a tissue sample of the designated tissue to undergo testing. If the tissue is determined as cancerous in early stages of cancer development, it can be removed before it develops into a late stage cancer and has the potential to grow drastically in size and or breadth — thereby making it difficult to breathe and severely limiting lung functionality — or further metastasize in the surrounding organs, increasing the fatality rate of lung cancer. In general, bronchoscopy is a pulmonary procedure that is often used to detect for tumors, obstructions, perform procedures such as foreign object removal or biopsies, perform stent implantation, or to perform select diagnostic treatments [15]. The bronchoscopy typically involves a pulmonologist inserting a bronchoscope through the nose or mouth, which has been numbed beforehand, and into the airways - known as the bronchial tree - until it reaches the desired location, at which point the designated procedure can be performed.

There are two types of bronchoscopes: rigid bronchoscopes and flexible bronchoscopes. Rigid bronchoscopes are often used when there are obstructions in the throat or airways, or if there is excessive bleeding in the lungs. This type of bronchoscope is generally larger in diameter and is most commonly used for foreign object removal and requires the patient to be anesthetized [16]. These scopes are generally not used in lung cancer detection and are often reserved for removing debilitating obstructions from the bronchial tract.

Flexible bronchoscopes are often used for early stage cancer detection as they are generally smaller in diameter than rigid bronchoscopes and are the preferred method for performing lung biopsies. These bronchoscopes are ideal for this type of procedure because they are able to traverse the bronchial tree to a greater degree than a rigid bronchoscope, and their flexibility provides them greater access to tissues that may be lodged at difficult to reach angles that require higher maneuverability. Furthermore, using this type of instrument is often preferred by pulmonologists for early stage detection as it is only minimally invasive with the

capability for greater control over the procedure as compared to needle biopsy procedures.

Also known as fiber-optic bronchoscopes, flexible bronchoscopes typically have a hollow channel - known as a working channel - through which instruments (such as forceps), irrigation, or fluids can be passed. These scopes often feature LED cameras that improve visualization for the pulmonologist during use [16]. An example of a flexible endoscope used in bronchoscopy for lung biopsy can be seen in Figure 1.1, where the black cylindrical tube is the endoscope, and the green tube that is exiting the working channel of the endoscope is the biopsy instrument (i.e. forceps) [1][2].

For this thesis, we will be using a flexible endoscope primarily designed for bronchoscopies that features an LED camera for visualization, and we will explore the design and implementation of a flexible robotic catheter to be used as an instrument with the flexible endoscope.

1.3 Previous Work

Industry Platforms

Several industry platforms have come to fruition with the aim to improve clinical outcomes for catheter-based procedures such as endovascular, bronchoscopic, and interventional electrophysiology procedures [4][5]. These platforms are often bulky and highly complex, such as the Auris Monarch platform (Fig. 1.2), Intuitive Surgical's Ion Endoluminal System, and the Hansen Medical Magellan™ 10 (Fig. 1.3) and Sensei™ X robotic platforms [4][3][17]. The Monarch™ Platform is designed for lung nodule-based bronchoscopic procedures, the Ion Endoluminal System is designed for lung biopsies and bronchoscopic procedures, the Magellan™ 10 focuses on endovascular procedures, and the Sensei™ platform is designed for electrophysiological procedures [4][17].

Hansen Medical also released a device following the Sensei™ robotic system called the Artisan Extend Control Catheter, which is designed to serve as an external steerable sheath to exert external control over a catheter placed within in

[4]. According to their website, the Artisan Extend Control Catheter is "designed to enable catheter stability, reachability and contact force sensing when navigating third-party catheters in electrophysiology procedures" [4].

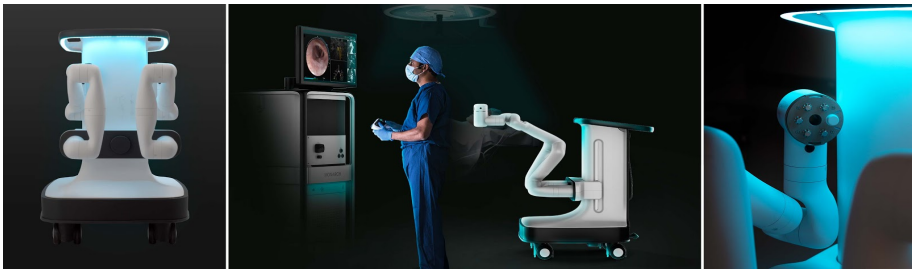

Figure 1.2: The Auris Monarch™ Platform [3].

These platforms have shown promise as safe methods capable of improving surgical outcomes, and the Auris Monarch™ platform was the first platform that achieved FDA clearance for bronchoscopic diagnosis and therapeutic treatment [4][17]. Since receiving FDA clearance, several certified doctors have performed successful cases that have been published as case studies by Auris Health, including lung biopsies, nodule diagnosis, tissue acquisition, and nodule dye-marking, in addition to approximately 1,000 additional cases by August 2019 alone [18][19][20][21][22][23].

The Monarch™ platform features an outer diameter of 5.7mm with a working channel of 4.4mm in diameter, which allows for larger surgical instruments to be passed through the channel [17]. Their instrument is fairly large in outer diameter as compared to several of their competitors, but this platform includes in that dimension a camera, suction, and irrigation to clear pathways for clear visualization and access to tissue for biopsies, which creates the potential for better surgical outcomes [3].

Following the Monarch™ platform's FDA clearance, Intuitive Surgical achieved FDA clearance for the Ion Endoluminal System in 2019. The Ion Endoluminal System uses preprocedural CT scans to perform guided bronchoscopy, focusing heavily on airway reconstruction and advanced control algorithms in their platform [17]. This platform features a 3.5mm outer diameter for its catheter, with a 2.0mm working channel [17], which is very similar to the catheter dimensions we are aiming to achieve through this work. A catheter with this outer diameter dimension is

able to traverse through smaller regions of the body and is ideal for procedures such as lung biopsies as it is capable of traveling sufficiently far into the bronchial tree.

Figure 1.3: The Hansen Medical Magellan 10 Platform [4][5]

The Magellan™ platform has been used in a variety of medical applications, some of which include Fenestrated Endovascular Aneurysm Repair (FEVAR) [24], treatment for nutcracker syndrome [25], and uterine arterial embolization in women [26], among a host of other cases and applications.

(a) Sensei™ X Robotic Catheter System [6]

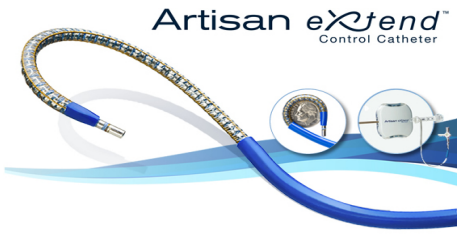

(b) Artisan Extend Control Catheter™ [7]

Figure 1.4: Created by Hansen Medical, (a) is the Sensei™ X Robotic Catheter System [6], and (b) is an Artisan Extend Control Catheter operated by the Sensei X and Magellan 10 platforms [7][5]

The Sensei™ Robotic Navigation System (RNS) (Fig. 1.4a) is a FDA approved platform primarily designed for laser ablation for cardiac procedures such as heart arrhythmias and arterial fibrillations (AF) [27][7]. It features a 3D joystick (seen in Fig. 1.3) that controls a steerable catheter sheath through which an ablation catheter can be passed [27]. This platform is designed to be used in conjunction with the Artisan Extend Control Catheter™ (Fig. 1.4b) produced by Hansen Med-

ical, or more recently the Lynx Catheter™, which is a flexible catheter designed for AF [7].

Table 1.1 outlines the procedures that each of the outlined platforms is designed for. This serves to show the diversity in catheter-based procedures that can be performed using a robotically-controlled medical device.

Table 1.1: Procedural Comparison across Platforms

Platform	Procedures
Monarch	Lung Nodule Bronchoscopy
Ion	Lung Biopsy & Bronchoscopy
Magellan 10	Endovasular
Sensei X	Electrophysiology
Artisan Control Catheter	Electrophysiology

While these platforms differ in application and design, they are the most prevalent robotic platforms available on the market that have FDA approval for medical use. For this thesis, we take a different approach to a catheter-based robotic platform designed for bronchoscopy, focusing on developing a device designed to by held and controlled by the specialist in the same room as the patient for the duration of the procedure.

Research Platforms

In this section, we will present several research-based developments in the realm of handheld devices for minimally invasive surgery. These developments may vary in scope to show the breadth of possibility within the medical robotics community.

While industry platforms have traditionally veered in the independent platform or mountable direction for catheter-based procedures and minimally invasive surgery, the research community has developed a range of handheld devices for use in various medical procedures, including minimally invasive surgery for percutaneous, bronchoscopic, and orthopedic procedures, among others.

We begin by looking at a handheld device outlined in a publication by K.E.Riojas et al. [8] that is used for minimally invasive surgery. Shown in Figure 1.5, their

device is not robotically actuated — instead, it uses a series of pull-wires and various other components oriented in a geometrical configuration that allow the wires to be mechanically manipulated. Their system uses mechanics and sensors to adequately store, measure, and release energy, thereby allowing for manipulation of the end-effector that is used to perform the procedures. This device has two degrees of freedom (DOF) in its "wrist" and two DOF in its "elbow," making is superior in terms of DOF to off-the-shelf bronchoscopes or other research-driven mechanically-actuated, non-robotic devices that offer one or two DOF [8]. Limiting the DOF allows for limited flexibility and directionality in what is typically a very confined, sensitive environment, so, while novel, this device has clear limitations compared to systems with higher degrees of freedom and increased modularity.

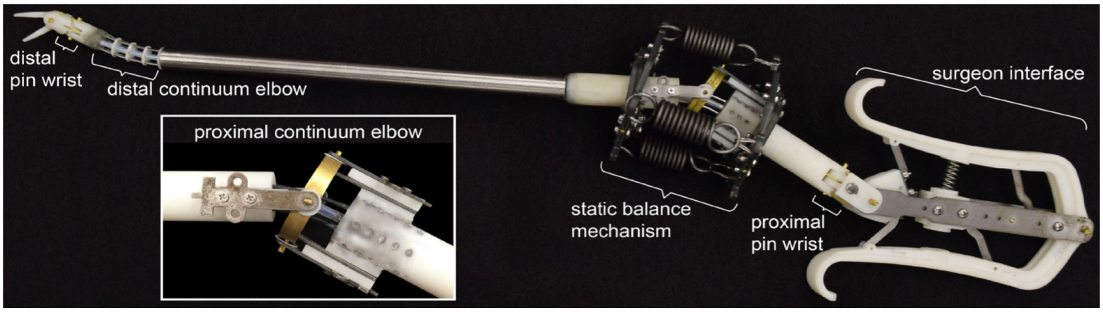

Figure 1.5: The non-robotic handheld device for minimally invasive surgery designed by Katherine Riojas et al. [8]

A noteworthy device that addresses some of these shortcomings has been developed at the University of California, San Diego in the Morimoto Research Lab. They propose a handheld concentric tube robot (CTR) to be used for minimally invasive surgical procedures, namely for percutaneous abscess drainage [9]. This CTR has attempted to remedy problems that mirror those for flexible bronchoscopes in that most available solutions that attempt to address the medically-relevant issues are mounted, teleoperated platforms rather than handheld solutions that pose as intuitive extensions of current procedures. The CTR they design offers increased directionality and control that better allows them to locate targets and perform procedures without requiring more involved surgery that results in more pain, recovery, and time lost for the patient [9].

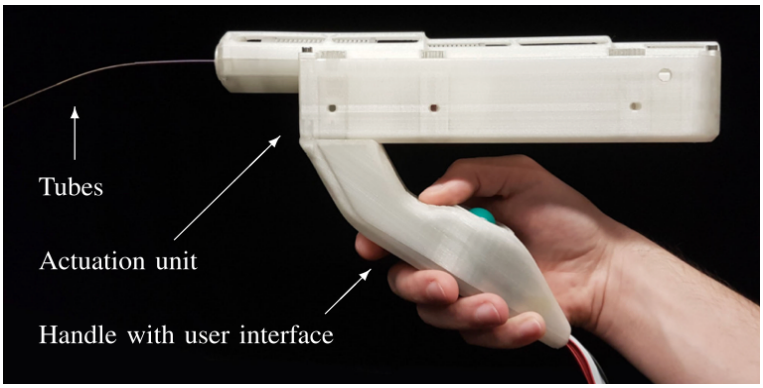

Figure 1.6: The handheld CTR device for minimally invasive surgery developed by Cedric Girerd et al. for the Morimoto Research Lab [9].

In addition to the device shown in Figure 1.6, CTRs are often used transorally for bronchoscopic procedures, so using this methodology to explore robotic solutions to difficult-to-reach (either due to distance or orientation) regions in the lung is not new. However, many of these devices are still in the research stage being evaluated as a tool for minimally invasive surgery. P.J. Swaney et al., for instance, have developed a transoral CTR that is designed to be combined with a steerable bronchoscope and a steerable beveled needle [10]. This combination of various steerable devices being used in tandem can offer several benefits: robotic device protection (bronchoscope acts as a sheath), additional orientational and directional degrees of freedom, and the potential for additional control over the location and path of the device *in vivo*. This is of note as this process of having several steerable devices that interconnect through the user will be the basis for the device we are proposing in this thesis.

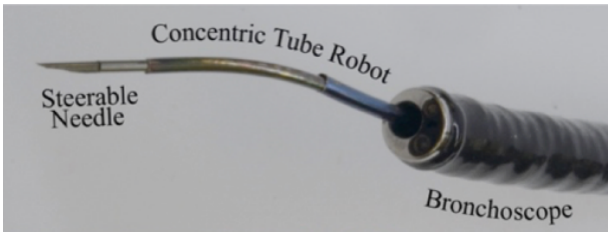

Figure 1.7: The handheld CTR device for minimally invasive bronchoscopic surgery developed by P.J. Swaney et al. [10].

Moreover, other groups have developed handheld devices for use in laparoscopic

surgery [28][29] and fetal surgery [30][31]. These devices are all novel in that they are handheld, often lightweight by nature of the handheld component, and to some degree flexible in their application. These components then can be broken down further and adapted to a broad range of medical procedures from bronchsocopy to laparoscopy to orthopedics, among many others. The main differences between these applications are the instrument being used to perform the procedure, the sheath that is being used to deliver that tool to its target destination, and the methods by which that sheath is manipulated. Next, we will introduce our contributions to this field as well as provide answers as to how we plan on addressing the list of variables for our specific application.

1.4 Contributions

Handheld, easily portable robotic catheter-based platforms are nonexistent in industry endoscopy. It is clear that the prior robotic catheter-based systems mentioned from Auris Health, Intuitive Surgical, and Hansen Medical primarily focus on large, mountable devices (the Sensei™ and Magellan™ systems) or platforms (such as the Monarch™ platform and the Ion Endoluminal System™) that are teleoperated either within the room where the platform is stationed or in a separate control room by a trained medical professional. We also saw that handheld devices that are being developed in the research community focus primarily on other procedures or else attempt to navigate the lungs and bronchial tree using concentric tube robots (CTRs) or some similar mechanism. Contrarily, the proposed platform outlined in this thesis is a handheld, catheter-based device. This device creates the opportunity for a simple, portable device that can be used in confined settings and does not require extensive training to operate as it is an extension of a familiar device used for bronchoscopy: a bronchoscope.

The platform outlined in this work focuses on portability, ease of use, lightweight feel, and modularity, meaning it can be adjusted easily to the user's specifications. Designed to be a robotically-controlled extension of devices surgeons are already familiar with (primarily bronchoscopes/endoscopes), it will allow for a surgeon to

perform a procedure with advanced imaging and controls without forgoing functionality. This leverages the skills surgeons develop to control endoscopes while also allowing for a user with less skill in controlling endoscopes to be able to manipulate the device. Its design is space-efficient and flexible as compared to industry platforms, basic endoscopes, or off-the-shelf catheters with limited sizes, directional capability, imaging capacity, and navigation control. The device features a modular 3D-printed casing that houses four lightweight motors and a joystick embedded in an ergonomically-designed, ambidextrous handle for straightforward catheter articulation. The catheter, which acts as a continuum robot with infinite degrees of freedom, protrudes outward from the casing. The flexible catheter can then be used in conjunction with an external flexible endoscope for increased flexibility, directionality, and imaging capabilities. Unlike similar teleoperated robotic platforms used for ablation as in [32], the handheld device allows the user to perform procedures on the patient in the same room, in real time, and with real time feedback and imaging.

Chapter 2

Design

2.1 Mechanical Design

This section details the mechanical considerations that went into designing the robotic handheld device. It will be divided into the following sections:

1. The design and manufacturing of the catheter.
2. The handle design and material.
3. The motor housing unit design and the relevant preloading and contact of the motors.
4. The current mechanical revision of the handheld robotic platform.

2.1.1 Catheter Design and Manufacturing

This section covers first the design of the catheter used in this work, followed by the stages of production involved in catheter manufacturing.

Design

The catheter used for this handheld platform features four tendons equally spaced around the perimeter of the working channel (inner lumen) throughout the entire length of the catheter to provide uniform deflection when pulled (Fig. 2.8).

The working channel of this catheter is 2mm (6Fr) in diameter, which allows for most standard surgical tools or instruments, such as surgical forceps and fiber optic lasers for ablations, used in catheter-based procedures to pass through the working channel to perform biopsies, laser ablations, or to inject liquids such as dyes or biomaterials through. To allow for optimal visualization, experiments featuring this catheter use a Misumi V1000LH Series camera with LED, 120° lens, and an outer diameter of 1.6mm. This camera is fed through the working channel to allow the surgeon to locate specific targets *in vivo*. Once the targets are located, the user can then remove the camera and feed an instrument or fluid through in its stead without having to move the catheter itself. Each tendon is attached externally to a motor via metallic interface components, and when the motors are turned, the catheter tip will deflect. These individual components will be explained further in the following sections.

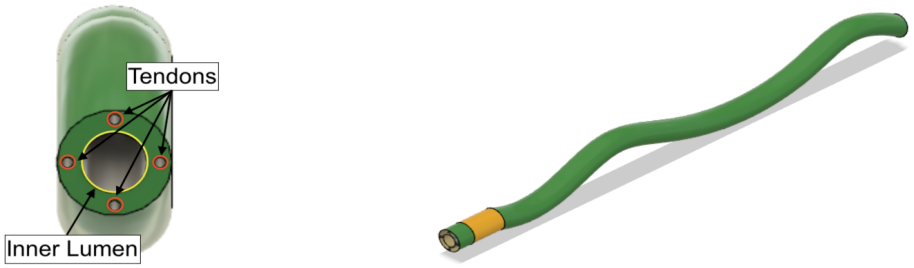

(a) Cross-Section (b) Longitudinal View

Figure 2.1: (a) Catheter cross section showing four equally-spaced tendons (red) surrounding the inner lumen (yellow), and (b) Longitudinal view of the body with a softer durometer (yellow, 52D) section for deflection and a stiffer durometer (green, 72D) section.

Manufacturing

The catheter used in this work, with a CAD replica shown in Figure 2.1, was manufactured in-house. The polyether block amide (Pebax™) jackets (72D and 52D durometer), fluorinated ethylene propylene (FEP) fusing sleeves, and Polytetrafluoroethylene (PTFE) liner used to manufacture this catheter are from Zeus Inc., and the polyimide tubing (0.0145" OD) used to align the four stainless steel tendons are from MicroLumen™. The PTFE-coated stainless steel mandrels used in the man-

ufacturing process to maintain the channels during heating were purchased from McMaster Carr (0.014" OD) and Component Supply Company (0.044", 0.045", 0.09" OD). The tool used to melt the components together to form a cohesive body is the BEAHM Designs Standard Hot Air System (Model 185-A). The final component in manufacturing the catheters are alignment pieces that were designed using SolidWorks and printed on the Formlabs Form 2 printer using Grey Pro Resin. These components can be seen in Figure 2.2.

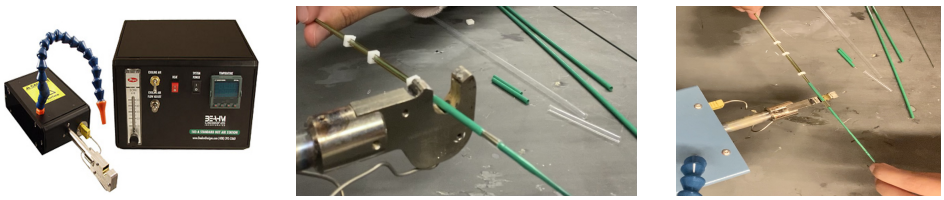

(a) Model 185-A (b) Side View (c) Top View

Figure 2.2: (a) is the BEAHM Designs Standard Model Hot Air System, (b) is a side view of the manufacturing process, and (c) is a top view of the manufacturing process.

The tendons are comprised of 0.009" stainless steel wires (Sava Cable, bare, 7x7 stranded stainless steel) that are aligned along the body by polyimide tubing. The catheter body is comprised of PEBAX, a heat-resistant, flexible polymer. When creating in-house catheter, two durometers were chosen to allow for end-effector articulation: a stiffer 72D PEBAX was chosen for the main body (shown in green in 2.1b), and a softer 52D PEBAX was chosen near the end effector (shown in yellow in 2.1b). By varying stiffness, more ideal articulation behavior is possible as the stiffness difference causes the softer material (52D) to articulate more readily than the stiffer material (72D). Finally, the inner lumen is lined with a PTFE liner that is heat-resistant, shrink-resistant, and lubricious, allowing for various instruments to pass through the channel with ease.

2.1.2 Handle Design

Early Revisions

Early revisions of the handle design can be seen in Figure 2.3. The handle itself is 3D-printed with a Markforge Onyx One desktop 3D printer using Onyx

material, which is a carbon fiber filled nylon material [33][34]. The handle is hollow, the material is lightweight, and the additional ergonomically-designed grip makes it comfortable to hold without adding significant additional weight.

The design in Figure 2.3a was altered due to the top-heavy nature of the device and lack of modularity. This design with motors held upright atop the handle was difficult to hold and very limiting as it did not allow the user the option to easily adjust the angle of the catheter for a given procedure. Instead, it would require dexterity on the behalf of the user to hold and angle the device simultaneously while also attempting to maintain the grip of a fairly bulky, top-heavy device.

(a) First Version (b) Updated First Version

Figure 2.3: (a) First motor housing revision with Maxon DC motors using a rubber strip to contain the various motor housing parts together, and (b) an early revision with an updated handle and motor housing design using the same Maxon DC motors.

These difficulties led to the design changes seen in 2.3b, which allows the user to alter the orientation of the motor housing and the catheter unit on the handle and adjust the angle of the orientation. The handle design orientation itself was flipped to allow the user to hold the device out in front of them, which made the grip more natural and comfortable. In this setup, the user can choose to place the motors in front of the handle to perform procedures that typically require horizontal insertion, or the user can place the motors on top of the handle with the catheter pointing down to perform procedures that are better suited for vertical insertion. This design and modularity is featured in the current revision of the

handle design.

Recent Revision

The handle is designed to be comfortable to hold for extended periods of time as surgeons may need to perform lengthy procedures requiring them to be able to hold the device for prolonged periods. To this end, the handle is made of the same 3D-printed Onyx material as the earlier versions and is designed to be hollow to decrease the overall weight and to allow for cable routing. Moreover, the handheld design is symmetric, meaning that it can be used ambidextrously. Furthermore, the handle attachment to the motor housing, which allows the user to choose the most comfortable position of the motors and motor housing on the distal end of the handle, which are connected via adjustable butterfly screws. This can be seen in Figure 2.4.

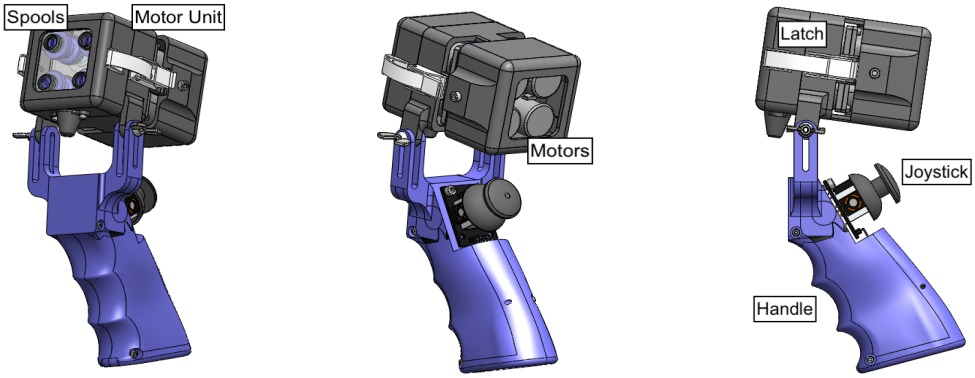

(a) Front View (b) Back View (c) Side View

Figure 2.4: Above is a labeled CAD rendering of the handheld with the current handle design and a recent version of the motor housing unit equipped with the current motors and spool set seen from multiple views.

Current Revision

The current revision of the handle is designed to be more modular than the previous versions. It is designed to clamp onto the Vathin endoscope and the handheld platform for a more modular interface that allows the device to be held in

one hand with the computer mouse to be held in the other hand. These components can be seen in Figure 2.5.

(a) Clamp (b) Wireless Mouse

Figure 2.5: This is the current handle design. It is comprised of (a) an adjustable clamp handle and (b) a wireless mouse.

Comparing Revisions

To compare these designs, we do a weight comparison as this is an important consideration in a handheld design. Ideally, the design is lightweight such that it can be held easily and comfortably for extended periods of time. The comparison can be seen in Table 2.1. The results from the table indicate that the handle and

Table 2.1: Weight Comparison of Handle Options

Combination	Weight
Handle + Joystick	59 g
Clamp + Mouse	379 g

joystick is the most lightweight while the clamp and mouse combination is heavier. In the future, there may be ways to reduce this weight, which would result in an optimal combination of lightweight feel with increased positional modularity as compared to the handle and joystick.

2.1.3 Motor Housing and Preloading

This section covers the early revisions and recent revisions of the encasing for the motors in the handheld device as well as the necessity for and design considerations involved in ensuring the motors are properly preloaded to ensure smooth functionality in the device control.

Early Revisions

The motor housing unit, shown above the handle in Figure 2.3a and to the right of the handle in Figure 2.3b, contains the motors as well as the connective components (spool cone and motor clamp components) that connect to the catheter. Early revisions of the motor housing can be seen in Figure 2.3. Although handheld, portable, and lightweight, the design in Figure 2.3a was altered due to the top-heavy nature of the device and the lack of modularity. This led to the design changes seen in 2.3b, which allows the user to place the motor housing to the location that is most comfortable to hold and alter the catheter location to that which is most convenient for their surgical purpose. This idea is replicated for the current revision, albeit there are some alterations to the design of the motor housing itself.

Early versions of the mechanical design explored preloading the motors using a metallic spring to improve the contact between the motor clamp and the spool cone (shown in Figure 2.6) at the interface between them. The springs were housed in the base of the 3D-printed motor housing design and are designed to push onto the motor base, thereby preventing slipping between these components. This design consideration is important because poor contact between the motor clamp and the spool cone would result in skewed articulation and could potentially damage the catheter tendons.

Recent and Current Revision

The motor housing unit, as labeled in Figure 2.4a for a recent version of the motor housing unit, contains the motors as well as the connective components (spool cone and motor clamp components) that connect to the catheter. The

(a) Separate Components (b) Fitted Together

Figure 2.6: (a) shows the spool cone (right) and the motor clamp (left) side-by-side, and (b) shows the two components fitted together.

top piece of the housing unit containing the spool cones and the top cover of the unit are removable and replaceable, requiring only a portion of the device to be sterilized for reuse (only the portion used in surgery and the pieces connected to it).

All motor housing unit components were chosen to be lightweight, natural to hold, and easily manipulable by the user. The design is modular, allowing the user to tune the angle and shift the motor weight to one of two main locations (floating above the handle with catheter pointing vertically downward or in front of the handle with the catheter pointing horizontally outward), both with additional angular positioning available (Fig. 2.8). The handheld housing is entirely 3D-printed, making it extremely lightweight and strong, with external latches for a fitted seal between the top catheter housing, which is removable, and the base motor housing. The top catheter housing is designed to be removable and replaceable as many catheters are designed for single-use purposes and would need to be disposed of after use. In this setup, the user would only need to remove the catheter and corresponding parts and replace those while all other parts of the handheld remain stationary.

To replace the necessity of preloading the motors in this revision, the current revision of the motor clamp and spool cone components are designed to prevent slipping via a spline. This design ensures that slipping is not possible as there will always be full contact between the motor clamp and spool cone, and these

Figure 2.7: Above is an early revision of the motor housing that used a rubber strip to contain the various motor housing parts together.

components are clamped together by an external latch that pressures the spools onto the motor clamp.

2.1.4 Mechanical Revisions

Recent Revision

A recent revision of the complete mechanical design can be seen in Figure 2.8. The handheld contains a recent version of the motor housing, ergonomic handle with joystick, and the catheter, as demonstrated in the labeled figure.

Current Revision

A current revision with the handheld base and catheter can be seen in Figure 2.9. This design is small in size and lightweight, with a sleeker profile than previous revisions. This design centered around a reduction in bulk and overall size, thereby increasing ease of portability. Additionally, it is designed to be compact, with the potential for the user to have more freedom and control over the angle and placement at the handheld-endoscope interface.

The weight breakdown of this design can be seen in Table 2.2.

(a) Physical Model (b) Labeled Rendering

Figure 2.8: (a) Physical robotic handheld catheter shown in downward facing orientation with motors floating above the handle and catheter protruding downward. (b) Labeled rendering containing primary features labeled for clarity.

Table 2.2: Weight Breakdown of Current Revision

Component(s)	Weight
Disposable Top (DT)	30 g
Handheld Base w/o DT	260 g
Handheld Base w/ DT	290 g

Comparing Revisions

To compare these revisions, we do a weight comparison as this is an important consideration in a handheld design. The comparison between the first version and the most current version can be found below in Table 2.3.

Table 2.3: Revision Weight Comparison

Revision	Weight
First Revision	448 g / 0.99 lbs
Current (C/M)	694 g / 1.53 lbs
Current (H/J)	365 g / 0.8 lbs

Figure 2.9: Above is the current revision of the handheld base without clamp that features the disposable top, motors, and motor housing on an upright, removable base.

As we can see from this breakdown, if the clamp and mouse (C/M) combination is selected with the most recent revision, the weight will be the greatest. However, this design contains a trade-off as it provides the most modularity and with an intuitive controller at a weight that is less than 2lbs total. If the handle and joystick (H/J) combination is selected, this results in the lightest option of those presented. This allows for a small range of options that can be selected based on the desired modularity and weight of the user.

2.2 Motor Selection

This section details the motors selected throughout various revisions in the development of this device.

Early Revisions

Early revisions of the handheld featured brushless direct-current (DC) and electronically communicated (EC) geared Maxon motors (seen in 2.10a and 2.10b/2.10c, respectively). These motors were selected for their simplicity of use and compatibility with Maxon motor drivers. These motors were replaced by Harmonic Drive motors in the current revision because the Maxon motors selected were too heavy

to comfortably hold and because they have nonzero backlash. Selecting motors with zero backlash was important because the functionality of the device requires highly fine-tuned control and precision.

(a) Maxon DC Motor (b) Earlier Maxon EC Motor (c) Recent Maxon EC Motor

Figure 2.10: (a) Maxon DC-powered motors used in first design. (b) Brushless Maxon EC motors used in early revisions. (c) More recent geared brushless Maxon EC motors used to validate the Maxon motor drivers.

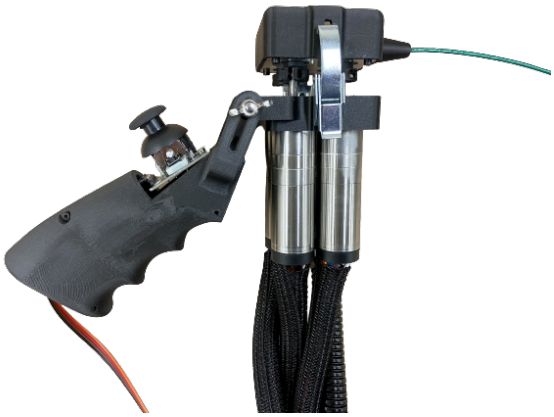

Figure 2.11: This is a recent revision using Maxon EC motors.

Current Revision

This design features Harmonic Drive RSF-5B-100-US 050-C supermini series brushless motors. These motors were chosen for their size-to-torque-output ratio, with a maximum torque output of 1.4 Nm with a length dimension of 58.1 mm, as referenced in Figure 2.12a.

(a) Individual Motor

(b) Full Motor Set

Figure 2.12: (a) An individual Harmonic RSF-5B-100-US 050-BC supermini series brushless motor including lengthwise measurement [11]. (b) This is a set of four Harmonic Drive RSF-5B Supermini Brushless 100:1 Geared EC Motors.

The Harmonic Drive motors are extremely small and lightweight, and they feature high precision motor control with zero backlash [11]. This is ideal for the finely tuned motion required in catheter articulation.

Comparing Motors

It is important to note that there is a difference in performance between brushed and brushless motors. Brushless motors allow for higher performance with increased controllability and a typically longer shelf-life as compared to brushed motors. For these reasons, in this work we transition from brushed DC motors to brushless motors as the designated motor type.

Additionally, to compare these different motors, we do a weight comparison as this is an important consideration in a handheld design. The comparison between the Maxon DC motors, the Maxon EC Max motors, and the Harmonic Drive supermini actuators can be found in Table 2.4 both individually (Ind) and as a set of four motors (Set).

The results from this table indicate that the Harmonic Drive motors are the lightest of the different motor types used throughout the prototyping process. Moreover, these motors are very high precision with no backlash, so there is no tradeoff with this motor and its performance. For these reasons, these are the motors that will be used in current and future revisions.

Table 2.4: Motor Weight Comparison

Motor	Weight (Ind)	Weight (Set)
Maxon DC	70 g	280 g / 0.6 lbs.
Maxon EC Max	209 g	836 g / 1.8 lbs.
Harmonic Drive	59 g	236 g / 0.5 lbs.

2.3 Hardware Components and Communication

This section outlines the hardware components that serve to manipulate the catheter end-effector. It will be divided into the following sections:

1. An an overview of how the motor driver boards were selected.
2. Using the Arduino Uno and thumb joystick hardware for interfacing between the user input and the motor driver boards.
3. PCB design for interfacing the Harmonic Drive motors with the Maxon EPOS2 modules.

2.3.1 Motor Driver Selection

Early Revisions

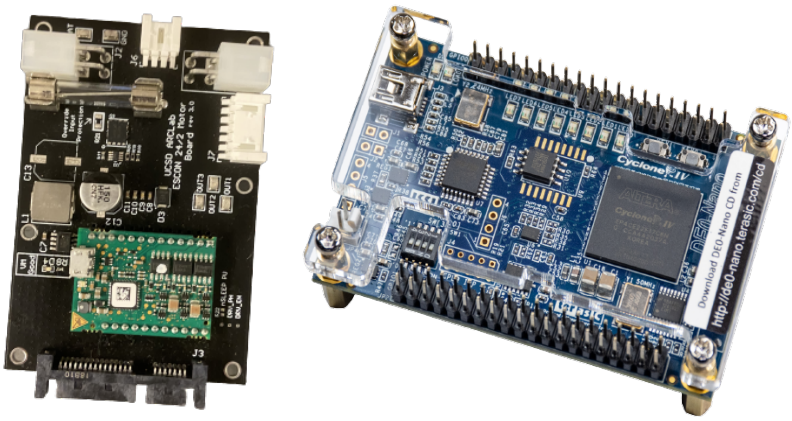

Figure 2.13: Here we have the custom board (left) and the DE0 Nano FPGA.

Early revisions of this device featured a set of custom motor driver boards designed by the UCSD Prototyping Lab in Atkinson Hall. These boards were created to communicate with a FPGA starter board known as the DE0-Nano. While this system was able to run on these boards early on using small DC-powered Maxon motors and later on EC-powered Maxon motors, due to the custom-designed nature of the board setup, it was prone to bugs that were not able to be solved rapidly. This generated lags in productivity, and the setup was fickle and cumbersome even while stationary, which is not ideal when attempting to create a reliable, easily portable system. This led us to find a more long-term, dependable solution in which each motor would connect to one motor driver. The motor controller is then linked to the other three drivers and easily connect to a computer via USB to avoid having to connect to the driver over Ethernet.

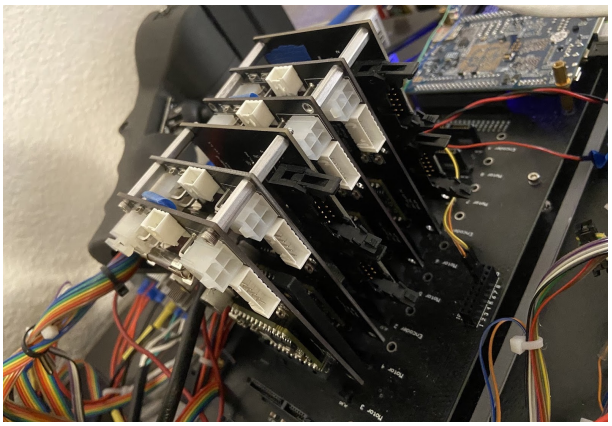

Figure 2.14: This is the original setup containing a set of four custom motor drivers connected via a large PCB to a DE0-Nano FPGA starter board.

Current Revision

In the most recent revisions, Maxon EPOS2 24/2 (Part number: 380264) EC position controllers (Fig. 2.15) were selected to control the motors. These controllers are ideal for their small size, easy to use interface, and control-friendly packages that allow for Robotic Operating System (ROS) communication. These controllers can be linked using CAN and USB, which allows for a simple setup that can be easily adapted to a large number of motors and inputs. By switching

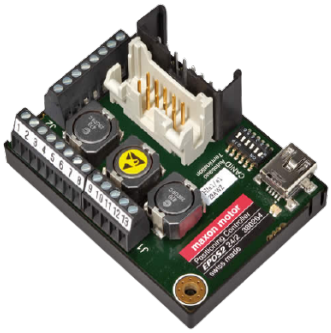

Figure 2.15: This is the Maxon EPOS2 24/2 EC Motor Driver used in the current revision.

over to these motor drivers instead of the custom boards, the system is now more easily portable, more robust in design, and is far easier to debug. A complete set of these drivers can be seen in Figure 2.16.

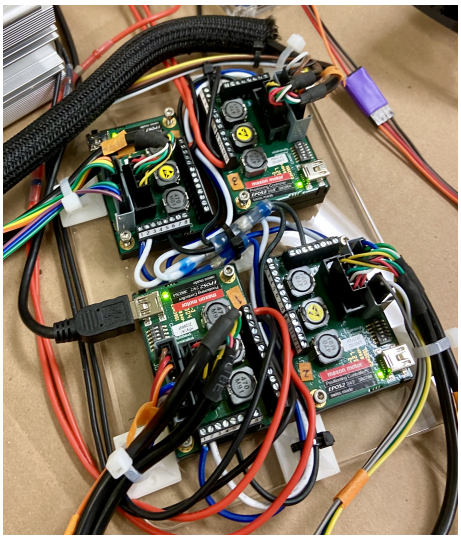

Figure 2.16: This is the current setup containing a set of four Maxon EPOS2 24/2 EC Motor Drivers bolted to an acrylic plate for ease of transport.

Comparing Motor Drivers

To compare these two systems, we do a weight and size comparison to determine ease of portability. The comparison between the DE0 Nano FPGA plus the custom motor driver boards and the Maxon EPOS2 modules can be found in Table 2.5 both individually (1), as a set of four motor drivers (4), and the total overall size

and weight (T).

Table 2.5: Motor Driver Size & Weight Comparison

Driver	Weight (1)	Size (1)	Weight (4)	Size (T)	Weight (T)
Custom	45 g	4”x2.5”	270 g	14.5”x4.25”	496 g
EPOS2	29 g	2”x1.5”	116 g	6”x4.75”	116 g

From this table, it is clear based on weight and size that the EPOS2 modules are more space-efficient and lighter compared to the custom solution. Moreover, because they are more intuitive to use with increased scalability and documentation, these motor drivers are ideal for a portable, evolving system such as the one presented in this thesis.

2.3.2 Arduino Uno and Thumb Joystick

In this work, an analog 5-pin thumb joystick (Product Code: MSM0000TJ) is used to control the motors and catheter and gives the user the ability to shift the catheter tip in any direction on the 360° circular plane. This allows for more control as compared to the levers or unidirectional or bidirectional knobs used in most off-the-shelf catheters and endoscopes. The joystick outputs get transmitted via ROS (as a publisher/subscriber) to the motor controllers, which respond by turning the motors accordingly.

Figure 2.17: This shows the thumb joystick.

To control the joystick, an Arduino Uno microcontroller board is connected to the joystick and the computer. The Arduino Uno reads and publishes the joystick motion to the computer, and the code subscribes to the publisher to determine the

necessary motor response. A more thorough explanation of the code can be found in Section 3.0.4, and tracing for the connection between the joystick and Arduino Uno can be seen in Figure 2.18 [12].

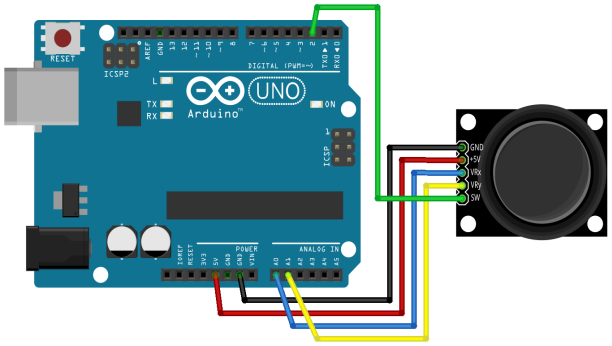

Figure 2.18: This shows the traces between the Arduino Uno microcontroller board and the thumb joystick [12].

2.3.3 PCB Design

The Harmonic Drive motors are incompatible with the Maxon EPOS drivers directly due to their low voltage signal, so a printed circuit board (PCB) is necessary as an intermediary for motor functionality. The PCB design contains three 4.7k resistors, each in series with power (VCC) and one of the three Hall effect sensor channels: A, B, and I. Known as a "pull-up," this raises the output signal of the motor channels to a level detectable by the motor drivers. The PCB also separates the incoming signal from the motors into two separate series: the three motor windings directly connect from the board to the driver without requiring any signal alteration, and the remaining five leads travel through the resistors that pull up the signal and then connect to a single-ended-to-differential Line Driver, which converts the 5-pin single-ended input signal to a 10-pin differential output as shown in Table 2.6. Due to the expected differential configuration on the driver boards, the L-Option (Avago) configuration was necessary for accurate mating with the driver board encoder connector. The L-Option configuration is a differential configuration — used less frequently than a standard differential pinout — with a pinout outlined in the 10-pin differential pinout column of Table 2.6.

The PCB was designed via Autodesk EAGLE, and the schematic can be found in Figure 2.19.

Table 2.6: Single-Ended to Differential (L-Option) Line Driver Pinout

5-PIN SINGLE-ENDED PINOUT		10-PIN DIFFERENTIAL PINOUT	
Pin	Description	Pin	Description
1	Ground (GND)	1	No Connection
2	Index (I)	2	+5V DC Power
3	A Channel (A)	3	Ground (GND)
4	+5V DC Power	4	No Connection
5	B Channel (B)	5	A- Channel (A-)
		6	A+ Channel (A+)
		7	B- Channel (B-)
		8	B+ Channel (B+)
		9	Index- (I-)
		10	Index+ (I+)

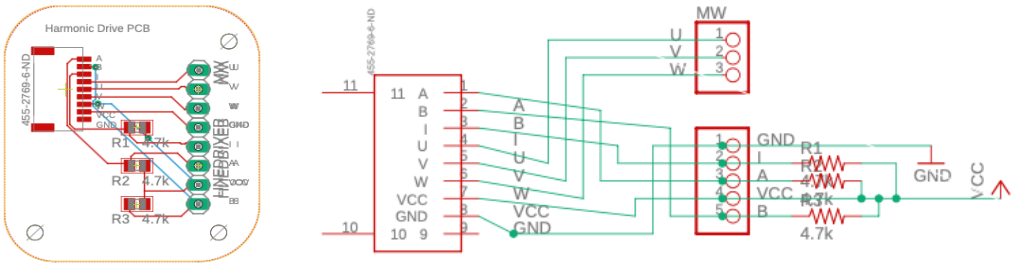

(a) Board (b) Schematic

Figure 2.19: (a) Autodesk EAGLE Board showing the dual layer leads with labeled connections, (b) containing equivalent schematic with labeled leads and connector formatting.

Chapter 3

Control

This details the control considerations that went into controlling the robotic handheld device. We will begin by including an overview of the communication between the joystick, motor drivers, and motors, before moving on to the mapping between these components. To accomplish this, this chapter will be divided into the following sections:

1. An an overview of the Robotic Operating System (ROS).
2. An an overview of EPOS Studio and the EPOS modules used to control the motors that articulate the catheter tip.
3. An an overview of the Arduino IDE control to read and publish joystick values to ROS.
4. And finally, the control mapping between the joystick and the catheter tip for articulation

3.0.1 ROS

Robotic Operating System (ROS) is a framework for writing software designed for robots using a single robust platform equipped with its own libraries and tools that make this communication between robots feasible and centralized. The novelty in this system lies in its contributors; ROS is a collaborative open-source framework in which anyone can contribute to the software development [35].

ROS functions primarily as a unidirectional messenger that allows messages to be passed between systems (inter-process communication), a process which often involves nodes, publishers, and subscribers [36]. A *node* is a computational process designated within a system, and multiple nodes can be used by different systems to communicate with one another via what is referred to as a ROS *topic*, which are essentially labeled buses [36][37]. These topics each then have their own associated publishers and subscribers. The *publisher* is usually a data generator that publishes the computation of the node, while a *subscriber* is interested in monitoring the data being published by the node publisher [36].

For the system outlined in this work, the communication between the motors, joystick, and controllers is handled through ROS. Through a series of publishers and subscribers, the joystick signal is published from the Arduino Uno to a ROS node, which is then interpreted and converted into motor movement by the drivers through subscribers written into the Python script in Linux. Using this communication allows for consistent and reliable catheter articulation.

3.0.2 EPOS Studio and EPOS Module

EPOS Studio

The Windows-based EPOS Studio graphical user interface (GUI) was used initially to verify motor functionality and also for debugging purposes throughout the process. The GUI is designed for select Maxon EPOS2 and EPOS4 drivers and can be found on the page of the driver the user is interested in. For the motor driver used in this work (EPOS2, Part Number 380264), the GUI download from the Maxon website for EPOS 2/4 drivers is found here [38].

In this GUI version, the user can program the motor drivers to the specific motor based on factors including commutation type, encoder resolution, gear ratio, and additional relevant information from the motor data sheet. In the case of the EPOS2 module used in this work, additional information includes the thermal constant, number of pole pairs, and the location of the gear on the motor. Once the correct values are inputted, the driver can undergo "Auto Tuning," which determined the optimal PID gains for the system by performing current, velocity,

and position control to determine optimal functionality. These parameters are then saved and stored by the driver. The interface allows the user to set up the motor/driver combination and verify functionality as well as determine whether the linking between motors is successful by allowing the user to control each motor individually as separate nodes. It can also be used to test position, profile position, velocity, profile velocity, current, and profile current control of each motor individually. Unfortunately, the interface cannot control all four motors at once, so external control that communicates with EPOS Studio are necessary to control all four motors in tandem.

To control the four motors simultaneously, the motors are initialized using the Maxon EPOS Linux Library — designed for initialization and communication in C++ — in Ubuntu. The Maxon EPOS Linux Library can be found here [38]. The packages allow the user to initialize each motor individually using encoder resolution, encoder polarity, and the gear ratio and to choose between position, velocity, and current control as the desired control method. This process manually initializes the motors based on the motor's individual data sheet using the same information as the Windows EPOS Studio GUI.

Once initialized, a Python script is used to write the control algorithms that will then be controlling the initialized motors. The specific mapping between the joystick and the motors and drivers is explored further in Section 3.0.5.

EPOS Module

3.0.3 Keyboard to Catheter Tip

To communicate between the motors and catheter tip, several control methods were developed, each designed for a different purpose with a different level of complexity. One of these methods of control is keyboard control, which is the first and simplest method of control. Four keys on the keyboard were designed to communicate with a motor pair to move in one of the four directions, with the control mapping shown in Table 3.1.

Table 3.1: Keyboard Control

Key	Position Change [x,y]
w	[0, +0.05]
s	[0, -0.05]
d	[+0.05, 0]
a	[-0.05, 0]

3.0.4 Arduino IDE and Joystick

The Arduino code changes the standard joystick reading from the range seen in Figure 3.1 to a more intuitive range, outlined in Table 3.2 [13].

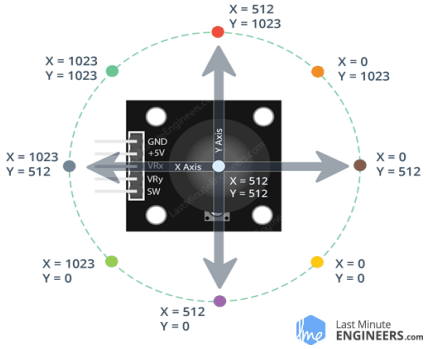

Figure 3.1: These are the inherent reading values from the joystick in the circular plane [13].

Table 3.2: Joystick Values

Old Value	New Value
0	-1
512	0
1023	1

Additionally, it creates a ROS publisher that publishes the joystick values, which the python script can then convert into motor pair movements that articulate the catheter in the designated direction. This designated directional pairing is covered more thoroughly in Section 3.0.5.

3.0.5 Catheter Mapping

Mapping between the control and catheter is coordinated using antagonistic pairs that correspond to the catheter tendon pairs. Two motors are designated to articulate the catheter in the up/down directions, while the other motor pair is designed to articulate the catheter in the right/left directions. Within this pairing, one motor spools to increase tension between the motor and the catheter pull-wire, resulting in the articulation, while the other motor spools to provide slack to the catheter channel to account for the increased tension between the other motor and the pull-wire, thereby preventing the catheter delamination or breakage while ensuring consistent motion along the catheter body and at the catheter tip. This method of tightening and releasing maintains tension as the catheter articulates, which allows for more fine motor movement as small changes in direction correspond to catheter tip articulation. Additionally, because the catheter maintains tension while articulating, the catheter response is prompt. A visual representation of this tensioning and releasing to cause articulation can be seen in Figure 3.2.

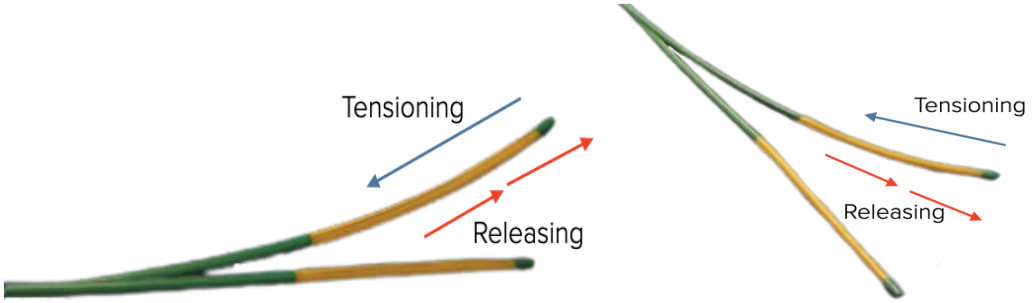

Figure 3.2: The tensioning and releasing directions for the left-direction and up-direction.

Inverse Kinematics

In flexible, continuum robot systems, there is an inherent non-linearity from hysteresis and friction that can serve to make a linear mapping difficult. There are various ways to mathematically model these phenomenon with the aim of addressing and counteracting them that go beyond the scope of this work. One prevalent system used to determine the kinematic equations for a tendon-driven continuum

robot, such as the catheter used in this thesis, is to combine two kinematic-based nonlinear models: the Cosserat rod and string models. This combined model is presented by Caleb Rucker and Robert Webster in [39] and can be used to better understand these behaviors.

For this work, we assume nonlinear effects are present at the catheter tip and represented using only one parameter: α, which will be represented further through another parameter: ϵ. As seen in Figures 3.4 and 3.5, α represents the difference between a neutral, centralized position of the catheter and full articulation distance. Because this value is difficult to measure and prone to inconsistency and error, we will not further attempt to examine this specific value. Instead, we will be analyzing the consistency of catheter tip articulation.

The mapping in this work that makes up the majority of the control scheme is done using inverse kinematics wherein a desired position is given and then the joint angles are calculated to reach that desired position. The equations that represent this dynamic are as follows, with parameters described in Table 3.3 and Equations 3.5, 3.6, 3.7, and 3.8:

$$\Delta d_{+x} = \theta_x(k_p + \epsilon_{+x}) + \text{offset} \tag{3.1}$$

$$\Delta d_{-x} = \theta_x(k_p + \epsilon_{-x}) + \text{offset} \tag{3.2}$$

$$\Delta d_{+y} = \theta_y(k_p + \epsilon_{+y}) + \text{offset} \tag{3.3}$$

$$\Delta d_{-y} = \theta_y(k_p + \epsilon_{-y}) + \text{offset} \tag{3.4}$$

The ϵ values are represented as follows:

Table 3.3: Inverse Kinematics Equation Parameters

Parameter	Description
$\Delta d_{+/-y}$	change in distance in y
$\Delta d_{+/-x}$	change in distance in x
k_p	proportionality constant
offset	initial tensioning offset
θ_x	angle of curvature in x
θ_y	angle of curvature in y

$$\epsilon_{+x} = \begin{cases} \alpha, & \text{if } \theta_x > 0 \\ 0, & \theta_x < 0 \end{cases} \tag{3.5}$$

$$\epsilon_{-x} = \begin{cases} \alpha, & \text{if } \theta_x < 0 \\ 0, & \theta_x > 0 \end{cases} \tag{3.6}$$

$$\epsilon_{+y} = \begin{cases} \alpha, & \text{if } \theta_y > 0 \\ 0, & \theta_y < 0 \end{cases} \tag{3.7}$$

$$\epsilon_{-y} = \begin{cases} \alpha, & \text{if } \theta_y < 0 \\ 0, & \theta_y > 0 \end{cases} \tag{3.8}$$

In equations 3.1, 3.2, 3.3, and 3.4, the *offset* refers to a value that is determined by initial tensioning. Because this is a tendon-driven robot with an interface between the catheter and spool, there is often slack in the tendon wire at this interface. If controlled with slack, the catheter will not articulate properly because when the spool tensions, it will not have enough pull at the onset to articulate the catheter. Because of this, it is important to pre-tension the catheter before inputting any controls, which will ensure that the catheter articulates properly with a given control input. Currently, this is done visually in an open-loop manner, so this value will vary each time the disposable top of the catheter is placed on the motor clamps and corresponds to the amount of cable that is wound around the spool before tensioning is complete.

To better understand the inverse kinematics equations visually in 2D, we can draw a point, as seen in Figure 3.3, and reference its θ values, θ_x and θ_y, along their respective axes.

A visual 2D representation of this applied to the catheter can be seen in Figures 3.4 and 3.5 below.

These images show the maximum articulation parameter α as represented through Equations 3.5, 3.6, 3.7, and 3.8 for ϵ. It also shows the direction in which θ_x and θ_y, or the angle of curvature in the x-direction and y-direction respectively, acts.

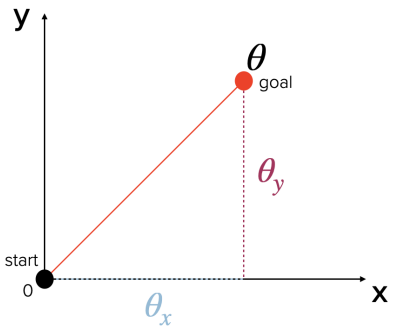

Figure 3.3: Visual axis representation of a point with its respective θ values.

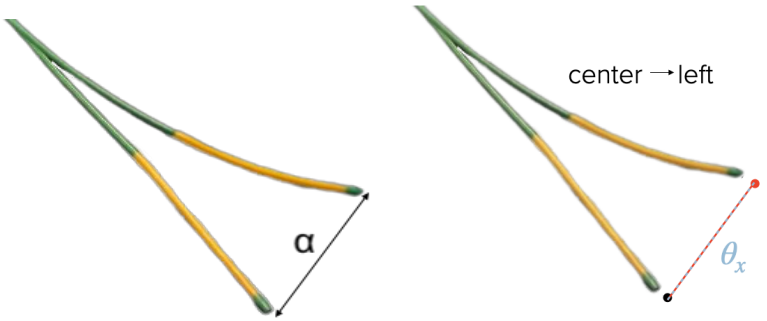

Figure 3.4: The difference between the neutral catheter position and the maximum articulation in the left-direction is represented by α through ϵ_x and θ_x.

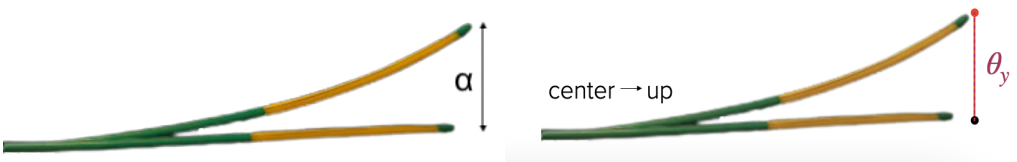

Figure 3.5: The difference between the neutral catheter position and the maximum articulation in the up-direction is represented by α through ϵ_y and θ_y.

Chapter 4

Experiments and Results

4.1 Catheter Biocompatibility Verification

This test was performed by Parker Pennington at the San Diego Zoo Safari Park's Beckman Center using a catheter segment made at the UCSD ARCLab. To determine whether the PTFE liner in the inner lumen is biocompatible and effective for passing biological material through without sticking or harmful interaction, a short, 6" segment of catheter was created and tested. With this shorter segment, several cat embryos and sperm were suspended in a medium and passed through the inner channel using a syringe. To determine whether there was sticking or interaction with the liner, the embryos were counted before injection and again after injection via a microscope. There was a total of 61 embryos passed through the catheter (Table 4.1), and, of those 61, 60 were successfully passed through while one was lost in the second set of trials. Of those 60 that made it through the catheter, four required two or more flushes before they exited the catheter. In total, this indicates that there was a 98.4% success rate of embryo recovery after the injection. This suggests that the PTFE liner is biocompatible and can be used to pass material such as embryos or sperm through the catheter without causing significant interaction or sticking with the liner. This test was performed over four separate trials, each varying several parameters seen in Table 4.1.

The first set of trials were control trials that used standard In-Vitro Fertilization (IVF), creating 35 total embryos and waiting five days until each embryo was at

Table 4.1: Catheter Biocompatibility Verification

IVF Type	Total Embryos	Embryos	Subcategory	Blastocysts	SP-EM
Control	35	17	CG	11	CG-CG
		18	EG	6	CG-EG
Catheter	26	12	CG	10	EG-CG
		13	EG	9	EG-EG
CG = Control, EG = Experimental (Catheter), SP = Sperm, EM = Embryo					

the 16+ cell stage. Of these 35 embryos in this trial, 17 were control embryos, created from control sperm and control embryos that had not interacted with the catheter before being passed through for the trial. The remaining 18 embryos were catheter embryos, which were created by using control sperm and embryos passed through the catheter early on in development before continuing maturation. The embryos were monitored for maturation after they were passed through the catheter to determine whether the interaction between the catheter liner and the early-stage embryo was harmful for the embryo maturation. The interaction does not appear to impact the embryonic development, as all of the embryos treated this way were able to reach maturation. In this trial, all of the catheter embryos were able to reach maturation and were successfully passed through the catheter without damage to the embryos (100% success rate).

The second set of trials were catheter trials using sperm that were all passed through the catheter before the trial and underwent standard IVF, creating 26 total embryos and waiting five days until each embryo was at the 16+ cell stage. Of these 26 embryos in this trial, 12 were control embryos, created from sperm that had previously been passed through the catheter and control embryos that had not interacted with the catheter before being passed through for the trial. The remaining 13 embryos were catheter embryos, which were created by using sperm that has been passed through the catheter before the trial and embryos passed through the catheter early on in development before continuing maturation. In this trial, all of the catheter embryos were able to reach maturation and all but one embryo successfully passed through the catheter without damage to the embryos (96.2% success rate).

There were several takeaways from this experiment. The catheter segment did not negatively or detrimentally impact the sperm or their function but did have a minor effect on embryo development. There is a possibility this minor detriment could be due to the catheter, or it could be that this resulted from the experimental methodology chosen. To pass the embryos through the catheter, including three minutes of incubation time, they required additional handling, which the control embryos did not require (although they experienced the same incubation time). This additional handling and physical movement of the catheter embryos versus the control embryos could explain the reduced development of the catheter embryos instead of the catheter liner being at fault. In this regard, more experimentation is necessary to determine the long-term impacts of the catheter materials on the desired biomaterials. This experiment was performed as an indicator of biocompatibility, and to this end the results indicate that the catheter is indeed biocompatible with low levels of sticking and damage to the biomaterials passed through with a high success rate of transfer.

4.2 Magnetic Tracker for Catheter Articulation Verification

This section covers the experiments performed with the robotic handheld catheter as they pertain to catheter articulation. In this section we present the following methods of characterization:

1. Desired Motor Position from the control input to the motors.

2. Hysteresis and Non-linearity characterization based on catheter articulation.

These sections will be covered both for a short catheter as well as a full-length catheter.

4.2.1 Short Catheter

Before performing experiments using a full-length catheter, a short catheter, measuring at approximately 6", was used to validate the experimental setup and

simplify the experiment. This catheter was manufactured in the same manner as the longer one, so we can expect the results to be comparable. Moreover, we expect the non-linearity and hysteresis effects to be lower in a short segment as opposed to a long one, where the potential for misalignment of the tendons is higher and the tendon length is far longer.

Desired Motor Position

In the initial experiment, we performed the experiment over the course of a complete trajectory in the positive and negative x and y directions in increments of 0.05 in a range from 0.0 to 1.0 for a total of 21 steps for complete deflection and 42 steps from rest to complete deflection back to rest. This was done using keyboard control, in which each direction correlates to a certain key on the keyboard, and each keyboard press moves the catheter in an increment of 0.05. With a consistent step input, we get the result seen in Figures 4.1 and 4.2.

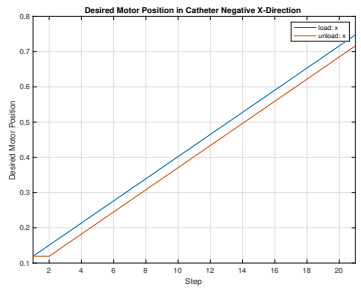

(a) X Input: -X Direction

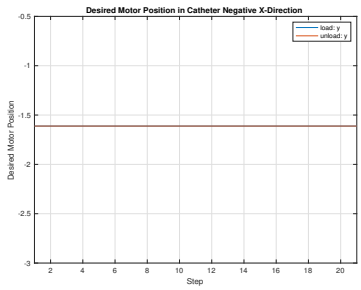

(b) Y Input: -X Direction

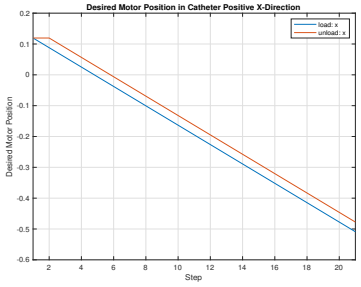

(c) X Input: +X Direction

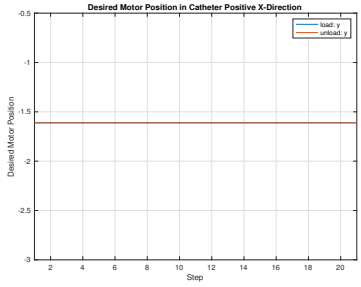

(d) Y Input: +X Direction

Figure 4.1: The plots show desired motor position sent from the keyboard to the motors. Plots in (a) and (b) are in the negative x-direction, (c) and (d) are in the positive x-direction.

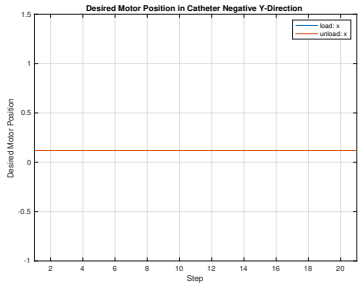

(a) X Input: -Y Direction

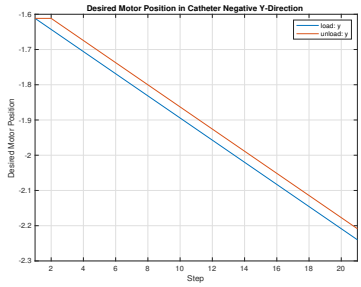

(b) Y Input: -Y Direction

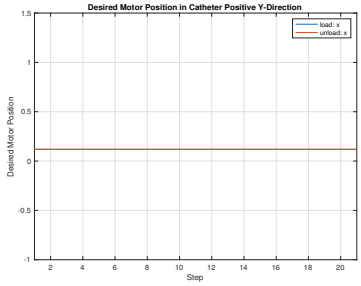

(c) X Input: +Y Direction

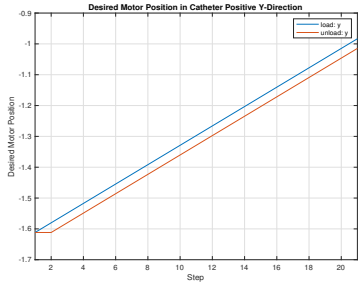

(d) Y Input: +Y Direction

Figure 4.2: These plots show the desired motor position that is being sent from the keyboard to the motors. Plots in (a) and (b) are in the negative y-direction, (c) and (d) are in the positive y-direction.

The results from Figure 4.1 lines up with intuition because there is no y-input in either of these directions, and the results from Figure 4.2 also aligns with intuition because there is no x-input in either of those directions, so there should not be any step input recorded.

Figures 4.1 and 4.2 show that the desired motor inputs correlate to the motor pairs responsible for a motion in a given direction. Furthermore, we see that the directional plots are opposites for the positive and negative directional pairings. Additionally, we see that when there is an input in the positive or negative x-direction, there is no movement sent to the motors in either y-direction, and conversely. This is important to note, as it indicates that any additional motion in either direction not correlated to motor input is likely due to a mixture of hysteresis and non-linear effects that prevent a one-to-one mapping from the motor input to the catheter tip articulation output. This phenomenon will be analyzed more closely in Sections 4.2.1 and 4.2.1.

Characterizing Nonlinearity: Raw Data

This work does not attempt to remedy or address nonlinear behavior, but it can be characterized through a magnetic tracker analysis to determine how hysteresis and tendon-sheath friction affects the catheter articulation. As this catheter is not perfectly elastic, we expect it to behave similar to a viscoelastic object with a clear loading and unloading curve that is not linear in nature. The results obtained from the raw, unprocessed, uncalibrated data can be seen in Figures 4.3 and 4.4.

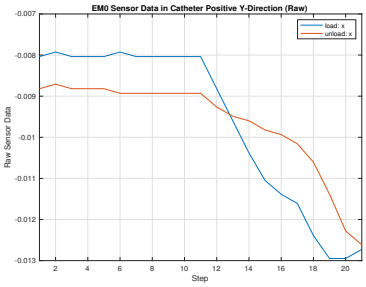

(a) Raw X Data: +Y Direction

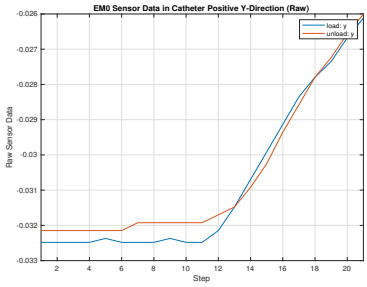

(b) Raw Y Data: +Y Direction

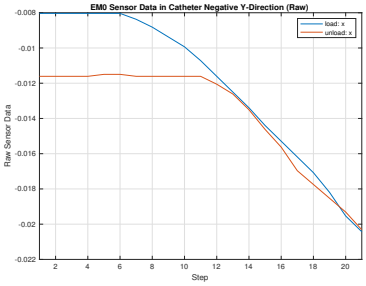

(c) Raw X Data: -Y Direction

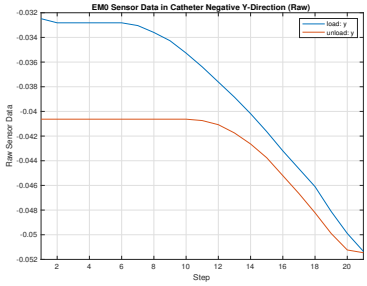

(d) Raw Y Data: -Y Direction

Figure 4.3: Raw magnetic tracking sensor data measured from the perspective of the magnetic tracker box. Plots in (a) and (b) are in the positive y-direction, (c) and (d) are in the negative y-direction. Hysteresis recorded during catheter articulation over 42 steps.

These plots show distinct loading and unloading curves that follow a similar trajectory to a viscoelastic, nonlinear material. In all of the plots, there is a period where no bending occurs followed by a near-linear period of bending, an apex, then a gradual, near-linear decline followed by a period of little-to-no bending before returning to a new zero position. This indicates that the material is not perfectly viscoelastic in nature, as the material does not experience a linear loading curve

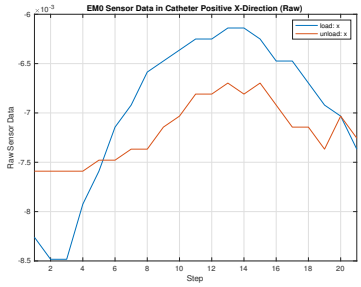

(a) Raw X Data: +X Direction

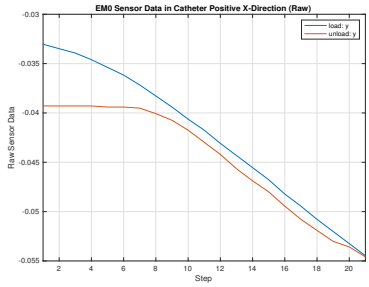

(b) Raw Y Data: +X Direction

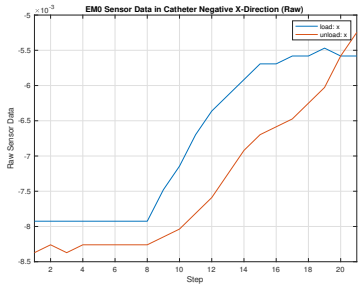

(c) Raw X Data: -X Direction

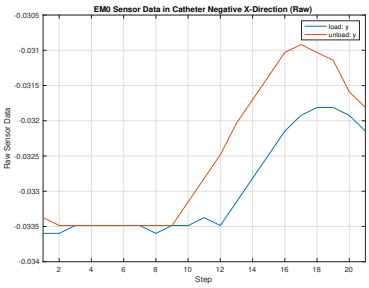

(d) Raw Y Data: -X Direction

Figure 4.4: Raw magnetic tracking sensor data measured from the perspective of the magnetic tracker box. Plots in (a) and (b) are in the positive x-direction, (c) and (d) are in the negative x-direction. Hysteresis recorded as the catheter articulates over 42 steps.

nor does it return back to the original zero point despite a control input that is designated as zero.

Characterizing Nonlinearity: Transformed Data

The data was recorded from the perspective of a magnetic field generator box. The raw, uncalibrated data from this perspective is presented in Section 4.2.1. However, we can calibrate and transform the data to determine whether the results match a visual interpretation of the bending. To do this, the points were transformed from the magnetic tracker box frame to a stereocamera frame that was used to visually track the catheter bending using the following equation:

$$P^C = R^{EM} P^{MT} + T^{EM}$$

where P^C is the point in the camera frame, P^{MT} is the point in the magnetic tracker frame, and R^{EM} is the rotation matrix and T^{EM} is the translation matrix

of the calibrated electromagnetic sensors from the perspective of the stereocamera. This relation gives us the points with respect to the camera frame, which allows us to more intuitively determine whether the results match a visual understanding of the behavior. The transformed 2D data from Figures 4.3 and 4.4 can be seen in Figure 4.5 and 4.6.

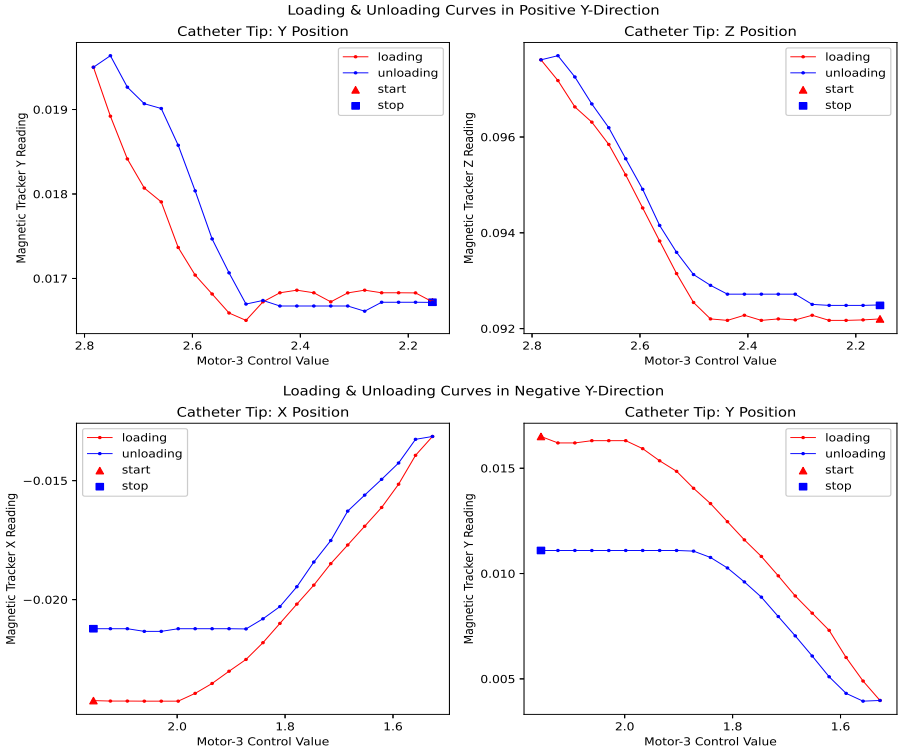

Figure 4.5: Transformed magnetic tracking sensor data measured from the perspective of the stereocamera. Plots show the loading and unloading curves in the positive and negative y-directions.

The transformed, calibrated data shows more clear loading and unloading curves that similarly follow the trajectory of a viscoelastic material. What can be noted from these results is that there is not a consistent zero position (the start and stop positions are not equal for most of the plots), which can be attributed to hysteresis and friction in the catheter. To determine whether this impacts the trajectory of subsequent trials, a trial showing repeating trajectories was performed.

The 3D trajectories of five subsequent trials can be seen in Figures 4.7 and 4.8. Each trial consisted of 42 steps total for a full range of motion, with 21 steps of

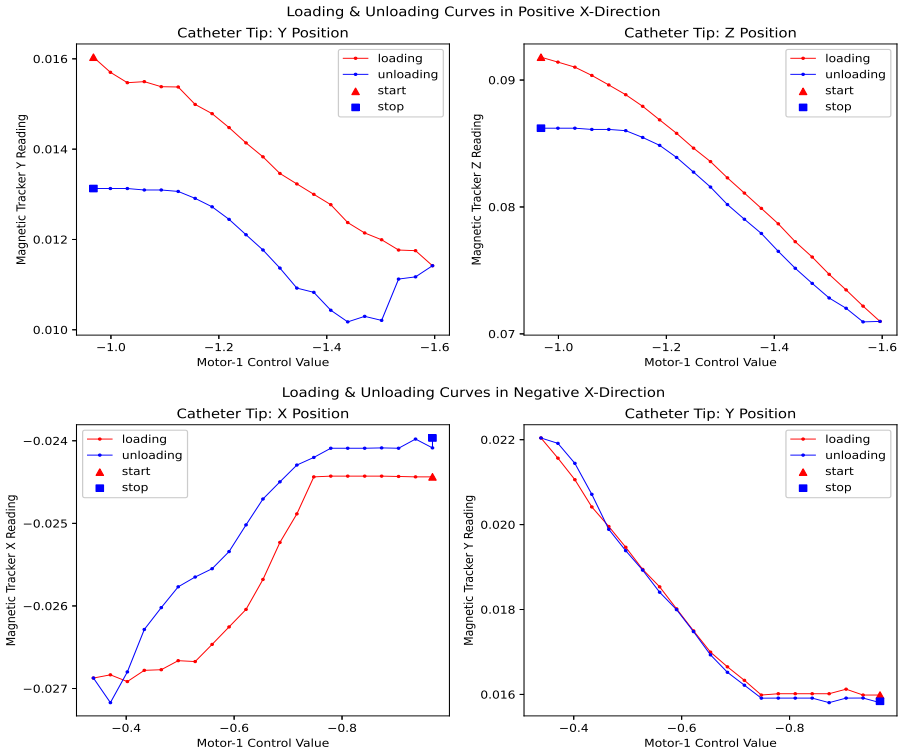

Figure 4.6: Transformed magnetic tracking sensor data measured from the perspective of the stereocamera. Plots show the loading and unloading curves in the positive and negative x-directions.

the ascending input from 0.0 to 1.0 in 0.05 increments and 21 steps of descending input from 1.0 to 0.0 in 0.05 increments. For clarity, each trial's starting point was mapped to that of the first trial to get a true understanding of trajectory.

As can be determined from the 3D trajectories, hysteresis and friction are responsible for slight variance between trajectories. It can be noted that each trial in each direction follows a very similar trajectory, which indicates that there is consistency in the path with consistent control input, but there is variance in the distance and height traveled at each input step. Initial tensioning likely also plays a role in these trajectories, causing some degree of differentiation in the different directions. The minimal hysteresis views also indicate that a majority of these nonlinear effects arise with respect to a combination of two axes, while another set of axes may not show such drastic nonlinear effects. This is worth noting for future work as it may help decide how to counteract or address the nonlinearity.

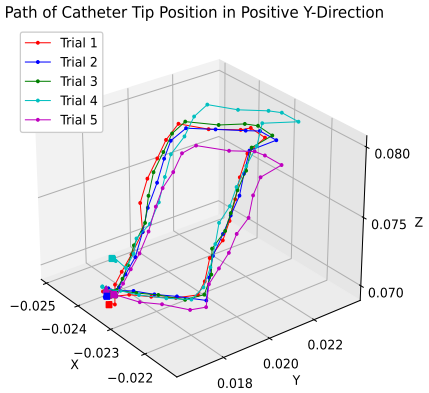

(a) Overview: +Y Direction

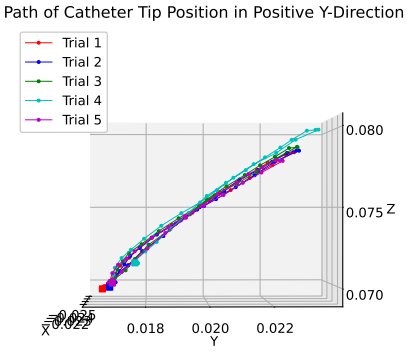

(b) Minimal Hysteresis: +Y Direction

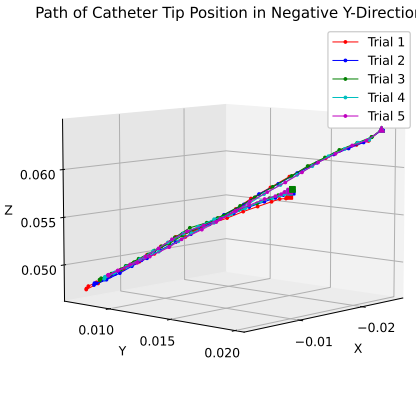

(c) Overview: -Y Direction

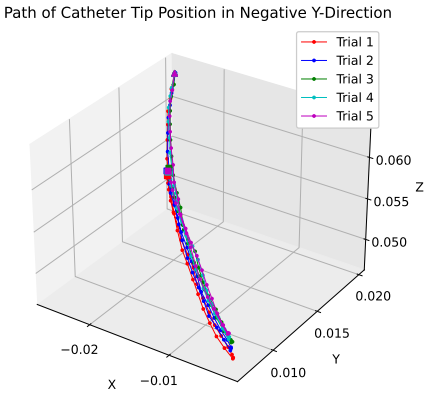

(d) Minimal Hysteresis: -Y Direction

Figure 4.7: Transformed magnetic tracking sensor data in 3D measured in the stereocamera frame. Plots (a) and (c) are the general trajectory overview, and (c) and (d) are the minimal hysteresis perspective.

4.2.2 Full-Length Catheter

For the full-length catheter (3ft.), the same repetitive trial was performed as with the short catheter to determine whether the nonlinearity due to hysteresis and friction is amplified in magnitude with a drastic length increase. The trials for this catheter were split into two categories: with endoscope and without endoscope. The trials where the catheter body is confined to an endoscope can be seen in

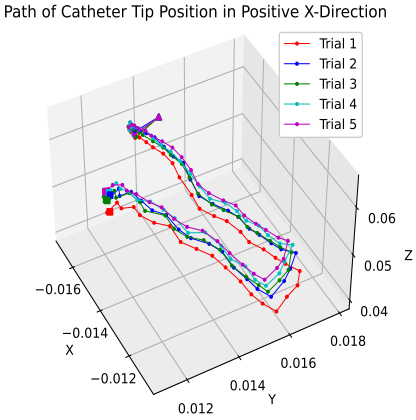

(a) Overview: +X Direction

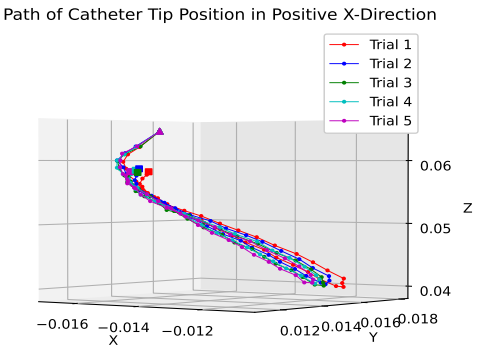

(b) Minimal Hysteresis: +X Direction

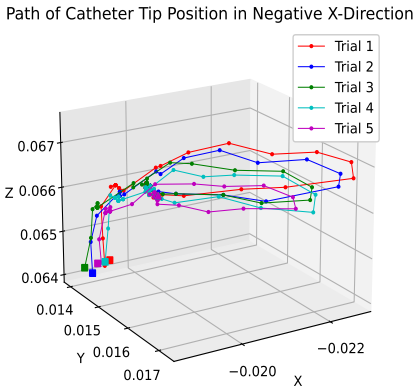

(c) Overview: -X Direction

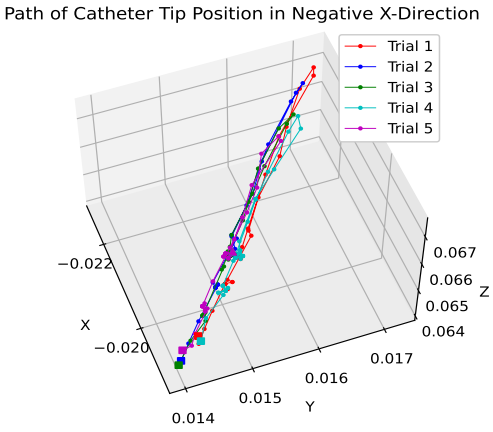

(d) Minimal Hysteresis: -X Direction

Figure 4.8: Transformed magnetic tracking sensor data in 3D measured in the stereocamera frame. Plots (a) and (c) are the general trajectory overview, and (c) and (d) are the minimal hysteresis perspective.

Figure 4.9c and 4.9d, while the trials where the catheter was not confined to an endoscope (free) can be seen in Figure 4.9a and 4.9b. The 3D plots from those resulting trials can be seen in Figures The 3D plots from those resulting trials can be seen in Figure 4.9.

These plots indicate that confining the catheter body via an endoscope does result in increased nonlinear behavior as there are distinct differences in trajectory

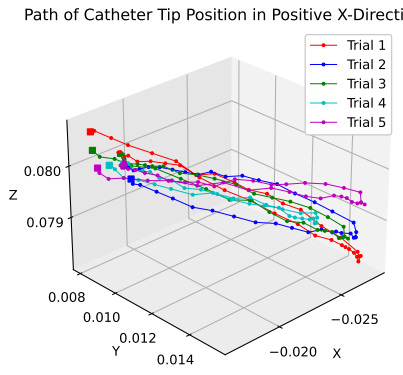

(a) Overview: No Endoscope

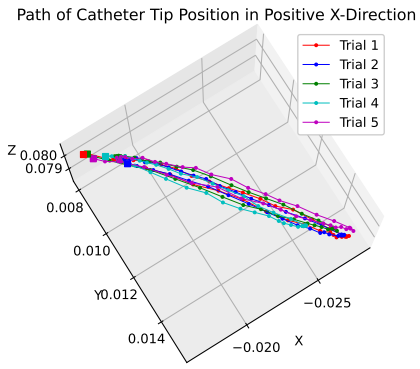

(b) Minimal Hysteresis: No Endoscope

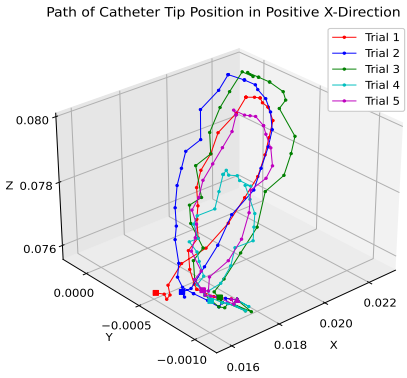

(c) Overview: With Endoscope

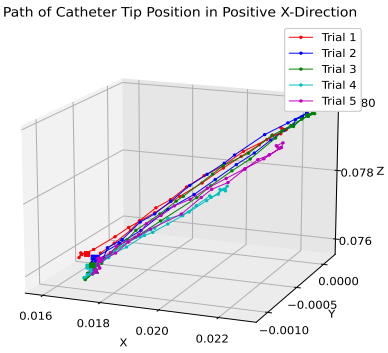

(d) Minimal Hysteresis: With Endoscope

Figure 4.9: Transformed magnetic tracking sensor data of full-length catheter in 3D measured in the stereocamera frame. Plots (a) and (c) are the general trajectory overview, and (c) and (d) are the limited hysteresis perspective.

and trajectory variance for the same control input. This aligns with intuition as there is increased friction in this system between the catheter body and endoscope channel in addition to friction between the tendon and the tendon sheath. This typically amplifies the nonlinearity as compared to the same experiment in free space. Regardless, there will be nonlinear behavior if the catheter is to be used *in vivo* as there would be friction between the catheter body and the tissue in an confined environment. In this scenario, the endoscope is likely a better tool that can be more easily remedied with lower repercussions than using the catheter

without an endoscope sheath limiting the motion of the catheter body.

4.3 Initial *In vivo* Experiments

For the purpose of these experiments, the bronchial tract was chosen as the desired focal area as the surgeon performing the experiments has expertise in this region. The robotic catheter was placed through a bi-directional, flexible Vathin 3.2mm working channel endoscope with an LED camera that would allow for increased visualization of the path. The catheter was fed through the working channel of the endoscope until it was just below the head of the scope, then it was inserted into the lung of a cadaveric pig. Once an ideal target location was determined, the catheter was fed through further until it was able to be visualized by the scope, then the catheter was articulated using motor controls (Fig. 4.10). Initial experiments indicate that the catheter can easily move through the *in vivo* tissue and is able to articulate inside a cavity.

This experiment was performed several times, and each time the catheter was able to articulate, even when the cavity was blocked and visualization was poor. This indicates that it will likely be able to traverse various types of anatomy with similar properties and degrees of visualization. However, this result is highly dependent on the skill of the user. More data is needed to determine whether this outcome is replicable and capable of performing a variety of procedures *in vivo*.

Figure 4.11 shows a tabletop version that has the same setup as used for the *in vivo* experiments. This setup contains a full-length catheter with motors and motor drivers. It was transported for this experiment and was able to be set up several times in different locations without issue.

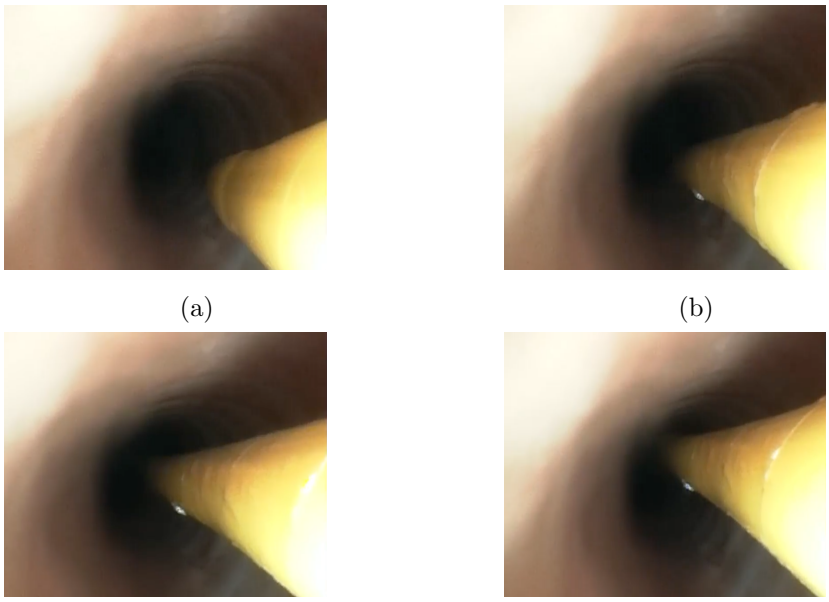

(a) (b)

(c) (d)

Figure 4.10: Catheter (shown in yellow) (a) entering the bronchial cavity in the lung, (b) at stationary base position at desired location, (c) moving toward roof of cavity, and (d) reaching roof of cavity via motor-controlled articulation *in vivo*.

Figure 4.11: The handheld system used for experiments equipped with a full-length catheter.

Chapter 5

Conclusion

5.1 Discussion and Future Work

The handheld robotic catheter is designed to aid surgeons in performing surgeries through an incremental process and is ideal for a broad range of catheter-based medical procedures. For the purposes of this thesis, we focus on bronchoscopy as a targeted procedure of interest to be used in lung biopsies. The working channel on this device can be used to pass various surgical instruments, such as forceps or ablation lasers, biological fluids, or small cameras through, among other possibilities, thereby allowing surgeons to perform specific procedures in various locations in the body with ease. As most surgeons that perform catheter-based procedures are adept at using endoscopes and catheters, this device is designed to be an extension of the tools they are already familiar with and includes additional imaging, modularity, and flexibility to further improve positive outcomes in these surgeries.

In the future, we will perform more experiments in cadaveric pigs to verify that the device can repeatedly and reliably perform procedures in highly complex, unseen environments requiring high dexterity, control, and visualization. Our future experiments also include tissue biopsies and laser ablations during bronchoscopic procedures to validate the system's capability to deliver positive outcomes. To this end, we will validate the catheter's ability to safely drive to various desired locations without damaging or otherwise compromising the tissue in the path, thereby endangering the patient.

Moreover, future work will attempt to remedy the nonlinear effects that arise from the inherent nature of a tendon-driven flexible system. This can be done in a variety of ways, one of which is to implement closed-loop control. To have a closed-loop system, we can add sensors that could include pressure, force, or tension sensing, or we could use fluoroscopy to track the catheter *in vivo*. Several works have looked into remedying friction, hysteresis, or nonlinearity in this type of tendon-driven system using a dynamic friction model [40], piecewise models [41], or deep learning models through long-short term memory (LTSM) [42][43], among many others. Additionally, several works have used a model-free approach to compensate for nonlinearity [44][45]. Any of these options may be used to remedy the nonlinearity in this system. Selecting which option is the best for this designated system will be left to future work.

5.2 Summary

With this work, we have shown the development of a handheld robotic catheter device to be used in surgery, namely bronchscopic procedures, to assist surgeons with procedures by providing increased directionality, control, and visualization. To do this, we designed a handheld, portable system that is low cost, intuitive, and simplistic, allowing for a system with a broad appeal and low overhead or required training. We have taken an incremental approach to this design so that it aligns with current methods that surgeons are already familiar with in an attempt to increase the appeal and adoption of such a device in industry. Initial experiments indicate that while there is still a necessity to address nonlinear effects including hysteresis and friction, this device has shown that it is capable of functioning in free space, confined space (via endoscope), and an *in vivo* environment while confined to an endoscope. These experiments indicate the great potential a handheld robotic device such as the one outlined in this thesis has as a medical device for catheter-based surgical and non-surgical procedures.

Appendix A

Additional Information

The hardware reference and physical measurements for the Harmonic Drive supermini actuator used in this work can be seen on the following page [11].

The hardware reference for the Maxon EPOS2 24/2 module can be found on the subsequent page [46]

RSF-5B-XXX-US050-C (Standard)

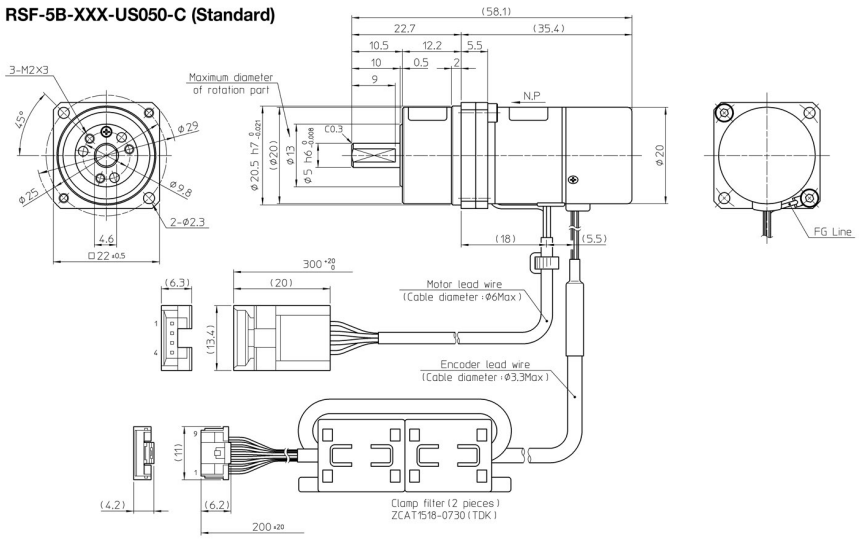

Harmonic Drive LLC
800-921-3332
www.harmonicdrive.net

4.1.4 EPOS2 24/2 for maxon EC motors (380264)

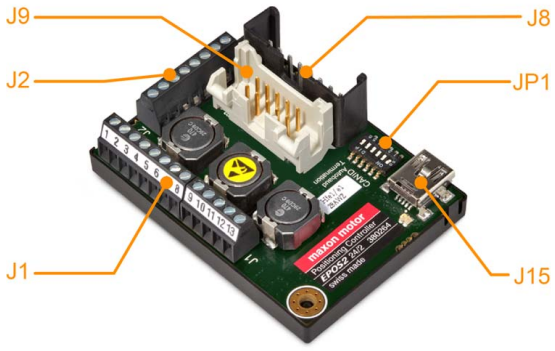

Figure 4-13 Interfaces – Designations and Location «EC» (380264)

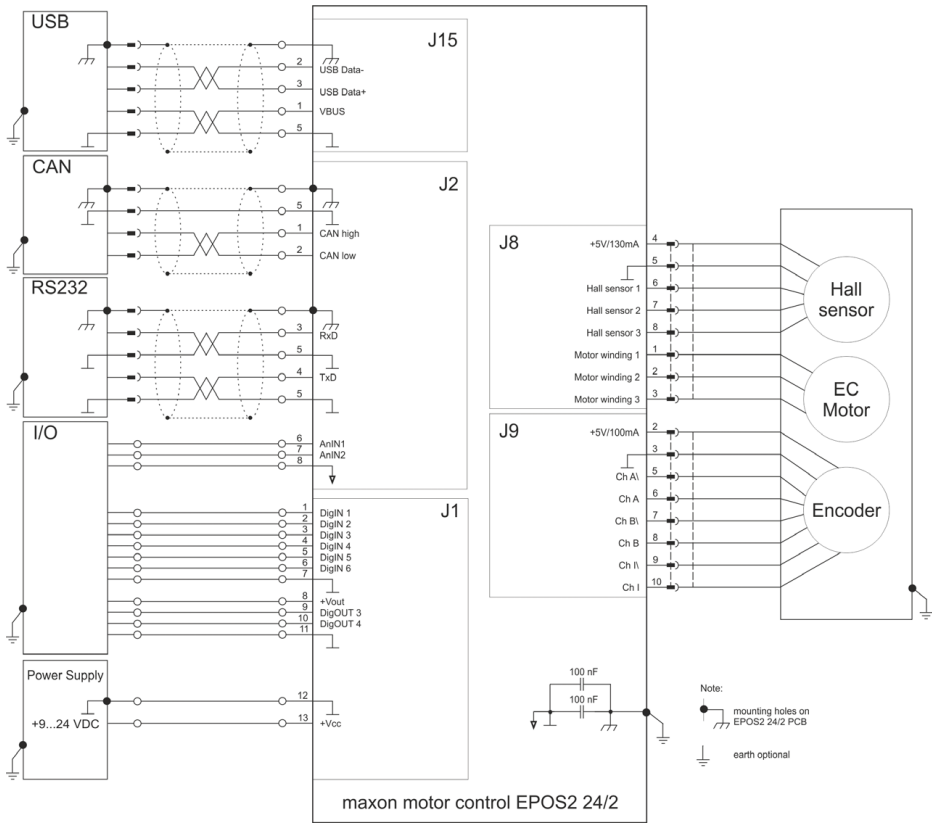

Figure 4-14 Wiring Diagram «EC» (380264)

Bibliography

[1] Thoracic surgery: Bronchoscopy mediastinoscopy — london health sciences centre.

[2] Basic bronchoscopy.

[3] Monarch platform - endoscopy transformed - auris health.

[4] Hansen medical - auris health.

[5] Fink Densford. Surgical robots: 11 companies you should know about, 2017.

[6] Magellan robotic system by hansen medical.

[7] Greg Galitzine. Hansen medical showcases robotic catheter system, 2009.

[8] Katherine E. Riojas, Patrick L. Anderson, Ray A. Lathrop, S. Duke Herrell, D. Caleb Rucker, and Robert J. Webster. A hand-held non-robotic surgical tool with a wrist and an elbow. *IEEE Transactions on Biomedical Engineering*, 66:3176–3184, 11 2019.

[9] Cedric Girerd and Tania K. Morimoto. Design and control of a hand-held concentric tube robot for minimally invasive surgery. *IEEE Transactions on Robotics*, 2020.

[10] P J Swaney, H B Gilbert, R J Hendrick, O Commichau, R Alterovitz, and R J Webster Iii. Transoral steerable needles in the lung: How non-annular concentric tube robots can improve targeting.

[11] Rsf supermini brushless servo actuator — harmonic drive.

[12] Analog joystick with arduino - tutorials.

[13] In-depth: How 2-axis joystick works? interface with arduino processing.

[14] Lindsey A. Torre, Rebecca L. Siegel, and Ahmedin Jemal. Lung cancer statistics. *Advances in Experimental Medicine and Biology*, 893:1–19, 2016.

[15] Bronchoscopy — johns hopkins medicine.

[16] Sandy Calhoun Rice. Bronchoscopy with transbronchial biopsy, 2018.

[17] Barbara Seeliger and Lee L. Swanström. Robotics in flexible endoscopy: current status and future prospects. *Current opinion in gastroenterology*, 36:370–378, 9 2020.

[18] Auris health celebrates 1,000 cases with the monarch® platform - auris health, 2019.

[19] Gustavo Cumbo-Nacheli. Peripheral nodule dye-marking with the monarch® platform, 7 2015.

[20] Kyle Hogarth. Diagnosis of 10mm eccentric lesion, 9 2019.

[21] Kyle Hogarth and Abhinav Agrawal. Diagnosis tissue acquisition for ngs of left upper lobe mass, 7 2020.

[22] Stephen Kovacs. Vision robotic control lead to peripheral nodule diagnosis, 6 2019.

[23] Justin Thomas. Successful biopsy of bilateral upper lobe apical lesions, 12 2020.

[24] Celia V. Riga, Colin D. Bicknell, Alexander Rolls, Nicholas J. Cheshire, and Mohamad S. Hamady. Robot-assisted fenestrated endovascular aneurysm repair (fevar) using the magellan system. *Journal of Vascular and Interventional Radiology*, 24:191–196, 2 2013.

[25] Fabien Thaveau, Philippe Nicolini, Benoit Lucereau, Yannick Georg, Anne Lejay, and Nabil Chakfe. Associated da vinci and magellan robotic systems for successful treatment of nutcracker syndrome. *Journal of Laparoendoscopic Advanced Surgical Techniques*, 25:60–63, 1 2015.

[26] Alexander Eric Rolls, Celia V. Riga, Colin D. Bicknell, Lesley Regan, Nick J. Cheshire, and Mohamad S. Hamady. Robot-assisted uterine artery embolization: A first-in-woman safety evaluation of the magellan system. *Journal of Vascular and Interventional Radiology*, 25:1841–1848, 12 2014.

[27] K. R.Julian Chun, Boris Schmidt, Bülent Köktürk, Roland Tilz, Alexander Fürnkranz, Melanie Konstantinidou, Erik Wissner, Andreas Metzner, Feifan Ouyang, and Karl Heinz Kuck. Catheter ablation - new developments in robotics, 12 2008.

[28] Francesco Focacci, Marco Piccigallo, Oliver Tonet, Giuseppe Megali, Andrea Pietrabissa, and Paolo Dario. Lightweight hand-held robot for laparoscopic surgery.

[29] Anderson PL, Lathrop RA, and Webster RJ. Robot-like dexterity without computers and motors: a review of hand-held laparoscopic instruments with wrist-like tip articulation. *Expert review of medical devices*, 13:661–672, 7 2016.

[30] H Yamashita, K Matsumiya, K Masamune, H Liao, T Chiba, and T Dohi. Two-dofs bending forceps manipulator of 3.5-mm diameter for intrauterine fetus surgery: Feasibility evaluation. *International Journal of Computer Assisted Radiology and Surgery*, 1, 2006.

[31] Wei Yao, Hariprashanth Elangovan, and Kypros Nicolaides. Design of a flexible fetoscopy manipulation system for congenital diaphragmatic hernia. *Medical Engineering and Physics*, 36:32–38, 2014.

[32] Prapa Kanagaratnam, Michael Koa-Wing, Daniel T. Wallace, Alex S. Goldenberg, Nicholas S. Peters, and D. Wyn Davies. Experience of robotic catheter ablation in humans using a novel remotely steerable catheter sheath. *Journal of Interventional Cardiac Electrophysiology*, 21:19–26, 1 2008.

[33] Onyx one fff 3d printer — markforged.

[34] Onyx - composite 3d printing material.

[35] Ros.org — about ros.

[36] Topics - ros wiki.

[37] Nodes - ros wiki.

[38] Online shop for high precise drive systems by maxon — maxon group.

[39] D. Caleb Rucker and Robert J. Webster. Statics and dynamics of continuum robots with general tendon routing and external loading. *IEEE Transactions on Robotics*, 27:1033–1044, 12 2011.

[40] Thanh Nho Do, Tegoeh Tjahjowidodo, Michael Wai, Shing Lau, and Soo Jay Phee. Performance control of tendon-driven endoscopic surgical robots with friction and hysteresis.

[41] Dong-Ho Lee, Young-Ho Kim, Jarrod Collins, Ankur Kapoor, Dong-Soo Kwon, and Tommaso Mansi. Non-linear hysteresis compensation of a tendon-sheath-driven robotic manipulator using motor current, 2021.

[42] Di Wu, Yao Zhang, Mouloud Ourak, Kenan Niu, Jenny Dankelman, and Emmanuel Vander Poorten. Hysteresis modeling of robotic catheters based on long short-term memory network for improved environment reconstruction. *IEEE Robotics and Automation Letters*, 6:2106–2113, 4 2021.

[43] D Wu, M Ourak, K Niu, Y Zhang, M Ahmad, J Dankelman, and E Vander Poorten. Towards modeling of hysteresis in robotic catheters based on lstm.

[44] Michael C Yip and David B Camarillo. Model-less feedback control of continuum manipulators in constrained environments. *IEEE TRANSACTIONS ON ROBOTICS*, 30, 2014.

[45] Mrinal Verghese, Florian Richter, Aaron Gunn, Phil Weissbrod, and Michael Yip. Model-free visual control for continuum robot manipulators via orientation adaptation. 9 2019.

[46] Epos2 24/2 hardware reference, 2017.